

Neutron Star Equation of State with Nucleon Short-Range Correlations: A Concise Review and Open Issues

Bao-Jun Cai^{1,2}, Bao-An Li³, and Yu-Gang Ma^{1,2}

¹*Key Laboratory of Nuclear Physics and Ion-beam Application, Institute of Modern Physics, Fudan University, Shanghai 200433, China*

²*Shanghai Research Center for Theoretical Nuclear Physics, NSFC and Fudan University, Shanghai 200438, China*

³*Department of Physics and Astronomy, East Texas A&M University, Commerce, TX 75429-3011, USA*

12/30/2025

Abstract

Nucleon short-range correlations (SRCs) and the associated high-momentum tail (HMT) in its momentum distribution $n(k)$ represent a universal feature of strongly interacting Fermi systems. In nuclear matter, SRCs arise primarily from the spin-isospin dependence of the tensor and short-range components of the nucleon-nucleon interaction, leading to a substantial depletion of its Fermi sea and a characteristic k^{-4} tail populated predominantly by isosinglet neutron-proton pairs. These microscopic structures modify both the kinetic and interaction contributions to the Equation of State (EOS) of dense matter and thereby influence a broad range of neutron-star (NS) properties. This short review provides a streamlined overview of how SRC-induced changes in $n(k)$ reshape the kinetic EOS, including its symmetry energy part and how these effects propagate into macroscopic NS observables, including mass-radius relations, tidal deformabilities, direct Urca thresholds and core-crust transition. We summarize key existing results, highlight current observational constraints relevant for testing SRC-HMT effects, and outline open questions for future theoretical, experimental, and multimessenger studies of dense nucleonic matter.

Keywords: *neutron stars; Equation of State; short-range correlations; high-momentum tails; nucleon momentum distribution $n(k)$; asymmetric nuclear matter; symmetry energy; mass-radius relation; tidal deformability.*

A Characteristics of single-nucleon momentum distribution $n_k^J \equiv n(k)$ with an SRC-induced HMT	1
B SRC-HMT Effects on Dense Matter EOS: Concise Overview of Main Findings	5
C SRC-HMT Effects on Neutron Star Properties: Selected Results with Open Issues	9
D Summary	16

A Characteristics of single-nucleon momentum distribution $n_k^J \equiv n(k)$ with an SRC-induced HMT

The Equation of State (EOS) of dense nucleonic matter is central to modern nuclear physics and astrophysics [1–34]. In particular, observables of neutron stars (NSs) reveal the EOS under extreme conditions including high densities and isospin asymmetries as well as strong-field gravity [35–37], where nuclear interactions become strongly correlated and naturally nonperturbative [38]. Among the microscopic ingredients shaping the EOS, nucleon short-range correlations (SRCs) and the associated high-momentum tail (HMT) in its momentum distribution function $n(k)$ have emerged as essential, experimentally established universal features of strongly interacting Fermi systems [39, 40].

SRCs originate from the strong short-range repulsion and tensor components of the nuclear force [42]. They deplete the Fermi sea and generate a universal $n(k) \sim k^{-4}$ tail at large k [43–45], confirmed in nuclei [46, 47], nuclear matter [48], and cold atoms [39, 40]. The tensor-dominated isosinglet nature of neutron-proton SRC pairs [46] induces a characteristic isospin inversion in asymmetric nuclear matter (ANM): majority nucleons dominate below k_F , while minority nucleons are overrepresented relatively in the HMT [46]. These correlated pairs possess large relative momentum and small center-of-mass momentum, predominantly back-to-back [49] as sketched in FIG. 1 and encode strong spin-isospin dependence tied to in-medium pion and ρ -meson dynamics [50–52]. In addition, SRC-HMT physics is known to influence the EMC effect [53–55], further demonstrating its wide relevance to nuclear medium modifications of nucleon structure functions.

*bjcai@fudan.edu.cn

†Bao-An.Li@etamu.edu

‡mayugang@fudan.edu.cn

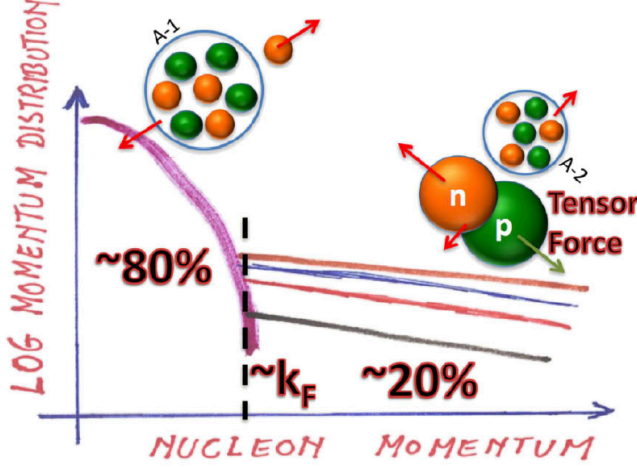


FIG. 1: (Color Online). A schematic illustration of the single-nucleon momentum distribution $n_k = n(k)$ in finite nuclei. Below the Fermi momentum k_F , nucleons predominantly occupy mean-field states, while above the Fermi surface, correlated neutron-proton pairs emerge due to the tensor component of the nuclear force. Figure adapted from Ref. [41].

Because the EOS depends sensitively on the nucleon momentum distribution, SRC-induced modifications of $n(k)$ directly affect the kinetic contribution to the EOS and the symmetry energy [56]:

$$\text{kinetic EOS: } E^{\text{kin}} \sim \int \frac{\mathbf{k}^2}{2M_N} n_{\mathbf{k}}^J d\mathbf{k} \sim \int dk k^4 n_{\mathbf{k}}^J = \int dk k^4 n(k), \quad (1)$$

here $J = n/p$ is the isospin index for neutrons/protons and $M_N \approx 939 \text{ MeV}$ is the static nucleon mass. These changes alter the pressure of neutron-rich matter, the parabolic approximation of the ANM EOS [57–61], nucleon effective masses [62], single-particle properties [63], and the composition of dense matter in NSs. Thus, SRCs and the HMT are not simply subleading corrections; they are structural components of a realistic, microscopically grounded EOS.

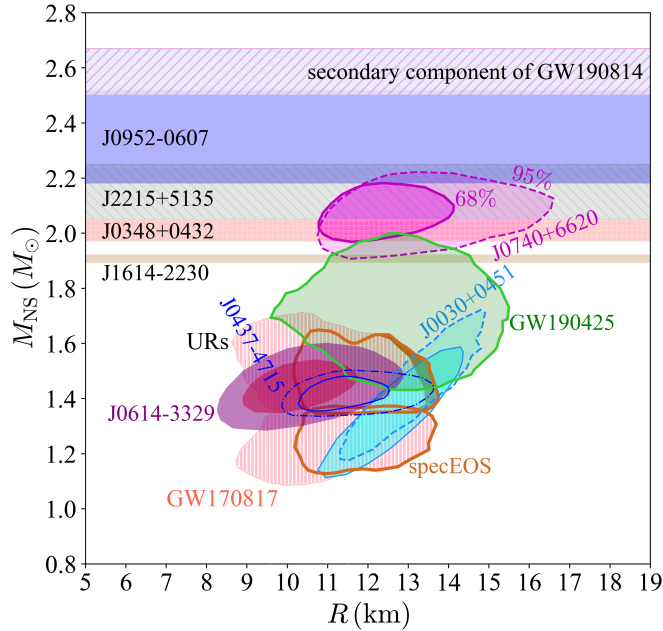


FIG. 2: (Color Online). A summary on NSs observed, these include the three GW events GW170817 [64,65], GW190425 [66] and GW190814 [67], the NICER mass-radius joint observations for PSR J0740+6620 [68], PSR J0030+0451 [69], PSR J0437-4715 [70] and PSR J0614-3329 [71], the joint X-ray and optical study of redback pulsar PSR J2215+5135 [72], the black widow pulsar PSR 0952-0607 [73], the mass of PSR J1614-2230 [74, 75] using Shapiro delay and mass of PSR J0348+0432 [76] via its spectroscopy.

The importance of these effects becomes amplified in NSs due to their large isospin asymmetry and high baryon densities. Consequently, the SRC-modified EOS influences the pressure-energy density relation underlying the NS mass-radius

(M-R) curves, tidal deformabilities, and the crust-core transition [37]. FIG. 2 summarizes current observational M-R constraints for several pulsars, these include the three GW events GW170817 [64, 65], GW190425 [66] and GW190814 [67], the NICER mass-radius joint observations for PSR J0740+6620 [68] (see also Refs. [77–81]), PSR J0030+0451 [69] (see also Refs. [82, 83]), PSR J0437-4715 [70, 84] as well as the recent announced PSR J0614-3329 [71], the joint X-ray and optical study of redback pulsar PSR J2215+5135 [72], the black widow pulsar PSR 0952-0607 [73], the mass of PSR J1614-2230 [74, 75] using Shapiro delay and mass of PSR J0348+0432 [76] via its spectroscopy; these observational data may guide how the SRC-HMT effects influence NS properties. The redistributed proton fraction associated with the HMT may shift the threshold for direct Urca cooling processes [85–87], while the altered single-particle spectrum and effective masses affect neutrino opacities, superfluid pairing gaps, thermal evolution, and transport coefficients [36]. At sub-saturation densities, SRC-driven modifications in $n(k)$ may influence the structure of neutron-rich clusters and nuclear pasta phases; at supra-saturation densities, they affect the stiffness of the EOS and thus the maximum NS mass, which is now tightly constrained about $\gtrsim 2.2 M_\odot$ [37] by astrophysical observations [68–84]. When combined with multimessenger constraints from NS binary-merger events [64–67], SRC-HMT physics provides a microscopic mechanism linking terrestrial nuclear measurements, many-body theory, and astrophysical probes of dense matter.

The aim of this short review is to highlight how SRCs and the HMT in $n(k)$ reshape the EOS of dense nucleonic matter and how these modifications propagate to NS properties. The review is organized as follows: the remainder of this section briefly discusses the structure of $n(k)$ with an SRC-induced HMT. Section B provides a concise overview of SRC-HMT effects on the dense-matter EOS; Section C presents selected results on SRC-HMT impacts on NS properties; we also highlight several open questions for future studies. Finally, Section D provides our concluding remarks. This short review mainly focuses on NS-related issues, and for broader discussions of SRC and HMT physics, the reader is referred to existing reviews, e.g., see Refs. [41, 88–99]. Given the limitations of the present authors' knowledge, this brief review is necessarily incomplete and may reflect certain biases in its coverage. Nevertheless, it is hoped that the materials presented here will provide a useful contribution to this rapidly evolving and fascinating field, in which many important and intriguing questions remain to be explored.

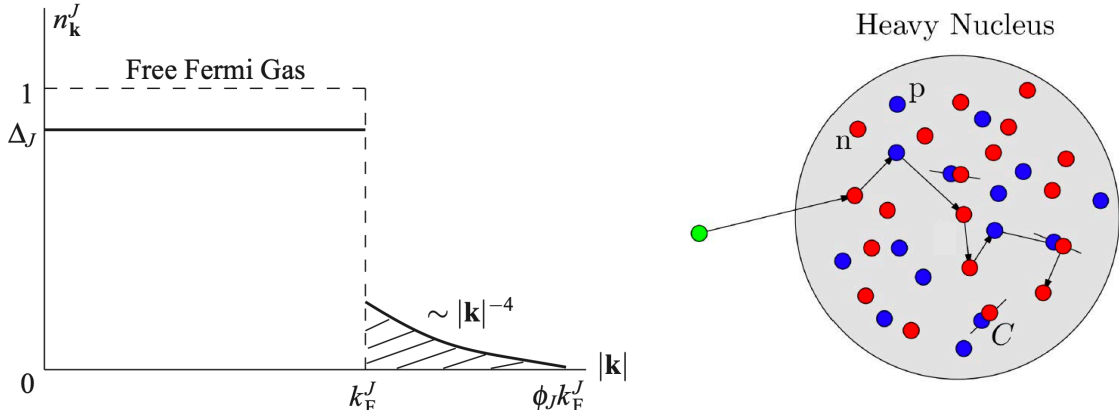


FIG. 3: (Color Online). Left: nucleon momentum distribution $n_{\mathbf{k}}^J$ in isospin ANM, showing the SRC-induced HMT above the Fermi surface and corresponding depletion below it. Figure taken from Ref. [100]. Right: the back-to-back configuration nature of high-momentum isosinglet neutron-proton pairs, which plays an essential role in shaping the EOS of dense matter and influencing related dynamical processes induced by the incoming projectile (green). Here, “C” characterizes the contact strength between an np pair.

The central feature of the single-nucleon momentum distribution $n_{\mathbf{k}} = n(k)$ in the presence of SRCs and tensor correlation is the emergence of a universal HMT of approximate k^{-4} form for $k_F \lesssim k \lesssim 2k_F$, accompanied by a depletion below the Fermi surface. A widely used parametrization is [100, 101]

$$n_{\mathbf{k}}^J(\rho, \delta) = \begin{cases} \Delta_J, & 0 < |\mathbf{k}| < k_F^J, \\ C_J \left(\frac{k_F^J}{|\mathbf{k}|} \right)^4, & k_F^J < |\mathbf{k}| < \phi_J k_F^J, \end{cases} \quad (2)$$

as illustrated in the left panel of FIG. 3. Here, $k_F^J = k_F(1 + \tau_3^J \delta)^{1/3}$ is the nucleon Fermi momentum with $k_F = (3\pi^2 \rho/2)^{1/3}$, as well as $\tau_3^p = -1$ and $\tau_3^n = +1$. The combined effects of SRCs and the tensor component of the nucleon-nucleon interaction give rise to back-to-back neutron-proton pairs (as shown in FIG. 1), which in turn can substantially modify the EOS of dense matter and influence the associated dynamical processes induced by a projectile (green), see the right panel of FIG. 3. The

corresponding high-momentum fraction of nucleon J in ANM, according to Eq. (2), is then given by [100–103]

$$x_J^{\text{HMT}} = 1 - \Delta_J = 3C_J(1 - \phi_J^{-1}). \quad (3)$$

Here Δ_J denotes the zero-momentum depletion, C_J the contact coefficient, and ϕ_J the effective HMT cutoff. Each parameter follows the generic isospin structure $Y_J = Y_0(1 + \tau_3^J Y_1 \delta)$ [101]. These coefficients are constrained by microscopic many-body calculations as well as analyses of electron- and proton-nucleus scattering experiments [43–46, 104–114]. Typical values include $C_0 \approx 0.161$, $C_1 \approx -0.25$, $\phi_0 \approx 2.38$, and $\phi_1 \approx -0.56$ [101]. The discontinuity at the Fermi surface, $Z_F^J = \Delta_J - C_J$, equals the inverse nucleon effective E-mass, as dictated by the Migdal–Luttinger theorem [62, 102, 104–106]. SRC-induced HMTs arise from complex in-medium nucleon-nucleon interactions, including the tensor force, and are probed not only in traditional electron- and proton-nucleus scattering [52] but also in nucleus-nucleus reactions [115]. The latter also includes experiments with rare-isotope beams in inverse kinematics. These measurements robustly support the approximate k^{-4} behavior up to $\sim 2k_F$ [46]. Understanding the microscopic origin of SRCs, their relationship to the EMC effect, and their broad implications for nuclear and astrophysical systems remains a central objective of ongoing and future experimental programs [116, 117]. Relevant efforts include SRC programs [118, 119] at the Electron-Ion Collider (EIC) at BNL [120], experiments by the R³B Collaboration [121, 122] at GSI-FAIR in Germany [123], and forthcoming campaigns at HIAF and the EicC in China [124, 125]. In addition, active SRC studies at Jefferson Lab, GSI, JINR, and IMP/Lanzhou continue to produce important results [126–129].

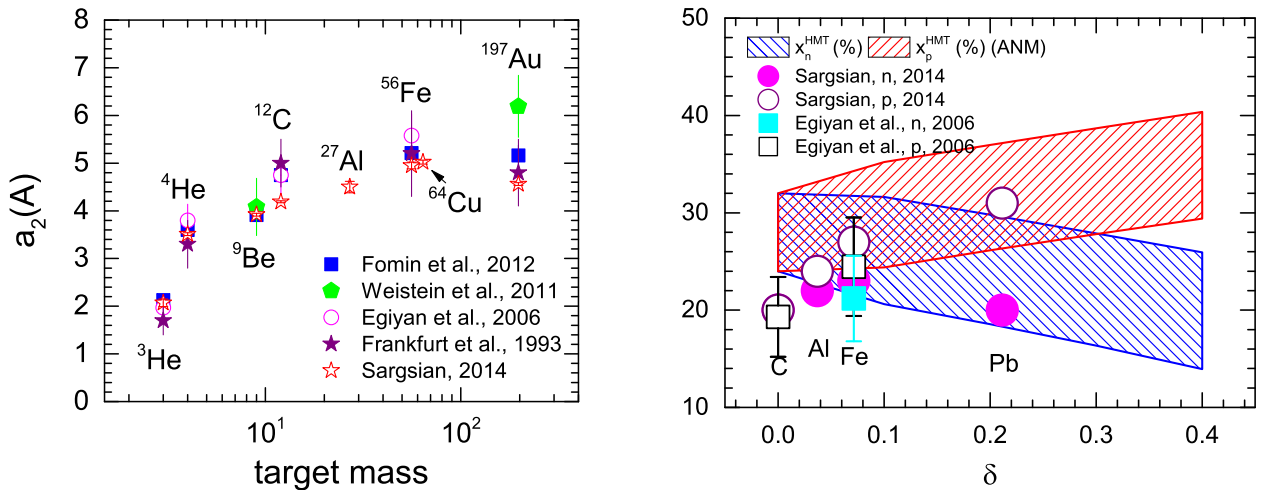


FIG. 4: (Color Online). Left: experimental $a_2(A)$ for several typical nuclei, i.e., ^3He , ^4He , ^9Be , ^{12}C , ^{56}Fe (^{64}Cu) and ^{197}Au [130–134]. Right: high-momentum nucleon fractions in heavy nuclei and nuclear matter. Figures adopted from Ref. [62].

When estimating the SRC-related coefficients such as C_0 , etc., a key empirical input is the high-momentum nucleon fraction in nuclear matter, which is typically inferred from measurements in finite nuclei. Based on microscopic calculations, the HMT of the nucleon momentum distribution is found to exhibit an approximate scaling from the deuteron to heavier nuclei, $n_{\mathbf{k}}^A = a_2(A)n_{\mathbf{k}}^d$ [95, 135–138]. Here $a_2(A)$ represents the relative probability of finding SRC-induced high-momentum nucleon pairs in nucleus A compared with the deuteron [96]. Experimentally, $a_2(A)$ is extracted from the plateau of the per-nucleon inclusive (e, e') cross-section ratios in the Bjorken-scaling region $1.5 \lesssim x_B \lesssim 1.9$ [90] as $a_2(A) = (\sigma_A/A)/(\sigma_d/2) = 2\sigma_A/A\sigma_d$. Representative values for ^3He , ^4He , ^{12}C , ^{56}Fe , and ^{197}Au are studied in Refs. [130–133] as shown in the left panel of FIG. 4, and extrapolation to infinite nuclear matter yields $a_2(\infty) \approx 7 \pm 1$ [114, 139–141]. Moreover, recent developments using the generalized contact formalism (GCF) provide a unified description of inclusive scattering at high x_B and momentum transfer Q^2 , reproducing the observed a_2 scaling patterns with realistic interactions [142–146]. These studies highlight that SRC-pair extractions carry $\sim 20\%$ uncertainties and require consistent treatments of nuclear structure and relativistic effects. As emphasized in Ref. [41], apparent inconsistencies in early SRC ratios [132, 133] mostly arise from mixing different experimental kinematics. The fundamental physics underlying the well-known linear EMC-SRC correlation [131] remains an open theoretical question [147, 148]. During the last decade, several theoretical frameworks have been benchmarked against the a_2 systematics [149–153]. For example, the self-consistent Green's function (SCGF) calculations [149, 154], using ratios of $\langle n_{\mathbf{k}}^0/n_{\mathbf{k}}^d \rangle_{\mathbf{k}=400-550 \text{ MeV}}$, yield $a_2(\rho) \approx b_1 \rho^{b_2}$ with $b_1 \approx 7-10$ and $b_2 \approx 0.4-0.5$, but their extrapolated saturation value underestimates $a_2(\infty)$ due in part to a lower high- k cutoff than used experimentally ($k \approx 300-600 \text{ MeV}$) [46]. Independent-particle-model (IPM) estimates [150, 151] based on the number of isosinglet pn spin-

triplet pairs predict an approximately linear rise of a_2 up to $A \approx 40$, followed by saturation, which is consistent with the data. Similarly, the low-order correlation operator approximation (LCA) [152] provides alternative estimates using the ratio or integral of $P^A(p)$ at large momenta, yielding total SRC scaling factors $\sim 4\text{-}5$ with non-negligible (pp, nn) contributions in addition to pn pairs. On the other hand, Quantum Monte Carlo (QMC) calculations with chiral EFT interactions [153] successfully reproduce the a_2 systematics up to ^{40}Ca and confirm the empirical EMC-SRC correlation for light nuclei. Their predicted saturation value, $a_2(A \rightarrow \infty) \approx 4.9\text{-}5.4$, is consistent with measurements on heavy nuclei. Experimental studies further indicate that reproducing both the deuteron D-state probability (4-5%) [96] and $a_2(\infty)$ requires an HMT fraction in symmetric nuclear matter (SNM) of $x_{\text{SNM}}^{\text{HMT}} \approx 28\% \pm 4\%$ [46, 114, 131, 132, 155–157]. In ^{12}C , about 20% of nucleons participate in SRCs, 90% \pm 10% of which are pn pairs [47, 132], corresponding to a pn-to-pp enhancement of ~ 20 , a pattern that persists for heavy nuclei [46]. By isospin symmetry, this implies a much smaller HMT fraction in pure neutron matter (PNM), $x_{\text{PNM}}^{\text{HMT}} \approx 1.5\% \pm 0.5\%$. Studies on extracting the a_2 factor and related issues are given in Refs. [158–165].

These empirical and theoretical findings indicate a pronounced isospin dependence of the HMT fractions x_J^{HMT} in ANM [46, 101, 134], with proton high-momentum fractions exceeding those of neutrons, as illustrated in the right panel of FIG. 4. Recent quasi-elastic (p, 2p) and (e, e'p) measurements in neutron-rich nuclei further quantify proton-neutron momentum asymmetries [160, 161]. Such constraints are essential for determining the coefficients C_0 and related parameters in microscopic EOS analyses, and consequently, precise knowledge of $a_2(\infty)$, x_J^{HMT} , and other SRC parameters is vital for constructing a reliable dense-matter EOS and interpreting multi-messenger observations of NSs.

Remarkably, despite the nearly 25 orders-of-magnitude difference in densities between nuclear matter and ultra-cold atomic Fermi gases, both systems exhibit very similar high-momentum tails with the universal $1/|\mathbf{k}|^4$ scaling. In both cases, short-range two-body correlations govern the large-momentum behavior: the tensor-force-induced np pairs in nuclei and the strong s-wave contact interactions in cold atoms. As a result, the probability of finding correlated pairs, quantified by the contact parameter, shows comparable magnitudes, highlighting an underlying universality in quantum many-body systems across vastly different scales [39, 40, 113].

B SRC-HMT Effects on Dense Matter EOS: Concise Overview of Main Findings

In this section, we briefly discuss the impact of an SRC-induced HMT on the EOS of dense matter, focusing on selected results from the literature; for a more detailed investigation, see Ref. [99]. As indicated by Eq. (1), the modification of $n_{\mathbf{k}}^J$ due to the SRC-HMT directly affects the kinetic EOS. Specifically, one has

$$E^{\text{kin}}(\rho, \delta) = \frac{1}{\rho} \frac{2}{(2\pi)^3} \sum_{J=n,p} \int_0^{\phi_J k_F^J} \frac{\mathbf{k}^2}{2M_N} n_{\mathbf{k}}^J(\rho, \delta) d\mathbf{k}, \text{ with respect to } \frac{2}{(2\pi)^3} \int_0^{\infty} n_{\mathbf{k}}^J(\rho, \delta) d\mathbf{k} = \rho_J = \frac{(k_F^J)^3}{3\pi^2}. \quad (4)$$

The left-hand side can be expanded as $E^{\text{kin}}(\rho, \delta) \approx E_0^{\text{kin}}(\rho) + E_{\text{sym}}^{\text{kin}}(\rho)\delta^2 + E_{\text{sym},4}^{\text{kin}}(\rho)\delta^4 + \dots$, defining respectively the kinetic EOS of SNM, the kinetic symmetry energy, and the fourth-order kinetic symmetry energy from left to right [101]. Using the $n_{\mathbf{k}}^J$ of Eq. (2), the first two terms are obtained as [101]

$$E_0^{\text{kin}}(\rho) = \frac{3}{5} E_F(\rho) \left[1 + C_0 \left(5\phi_0 + \frac{3}{\phi_0} - 8 \right) \right] \equiv \frac{3}{5} E_F(\rho) [1 + C_0 \Phi_0], \quad (5)$$

$$E_{\text{sym}}^{\text{kin}}(\rho) = \frac{1}{3} E_F(\rho) \left[1 + C_0 (1 + 3C_1) \left(5\phi_0 + \frac{3}{\phi_0} - 8 \right) + 3C_0 \phi_1 \left(1 + \frac{3}{5} C_1 \right) \left(5\phi_0 - \frac{3}{\phi_0} \right) + \frac{27C_0\phi_1^2}{5\phi_0} \right], \quad (6)$$

where $E_F(\rho) = k_F^2/2M_N$ is the nucleon Fermi energy in SNM. The second equality in Eq. (5) defines the factor Φ_0 , which is greater than 1 due to $\phi_0 > 1$. The SRC-modified kinetic EOS has two main consequences [101]:

- (a) The factor inside the brackets of Eq. (6) is negative, indicating that the kinetic symmetry energy is significantly reduced by SRC-HMT, despite the enhancement of the kinetic EOS of SNM.
- (b) The full EOS of ANM $E(\rho, \delta) = E^{\text{kin}}(\rho, \delta) + E^{\text{pot}}(\rho, \delta)$ generally includes a potential contribution $E^{\text{pot}}(\rho, \delta)$. To maintain consistency with empirical constraints around saturation density [166], the potential part (either of SNM or of the symmetry energy) must readjust correspondingly. This leads to changes in the density dependence of the EOS, which can have sizable effects on NS properties. Similarly, Eq. (4) can be generalized in two ways:

(1) Including relativistic corrections to the nucleon kinetic energy gives [167]

$$E^{\text{kin}}(\rho, \delta) = \frac{1}{\rho} \frac{2}{(2\pi)^3} \sum_{J=n,p} \int_0^{\phi_J k_F^J} \frac{\mathbf{k}^2}{2M_N} \left(1 - \frac{\mathbf{k}^2}{4M_N^2} + \frac{\mathbf{k}^4}{8M_N^4} - \frac{5\mathbf{k}^6}{64M_N^6} + \dots \right) n_{\mathbf{k}}^J(\rho, \delta) d\mathbf{k}. \quad (7)$$

(2) Including effective mass corrections yields [100]

$$E^{\text{kin}}(\rho, \delta) = \frac{1}{\rho} \frac{2}{(2\pi)^3} \sum_{J=n,p} \int_0^{\phi_J k_F^J} \left(\sqrt{\mathbf{k}^2 + M_N^{*,2}} - M_N^* \right) n_{\mathbf{k}}^J(\rho, \delta) d\mathbf{k}, \quad (8)$$

where M_N^* is some type of the nucleon effective mass [62].

In both cases, the potential part should adjust consistently with the kinetic contribution.

More generally, when evaluating any quantity affected by the SRC-HMT, the following prescription applies. For an arbitrary function f at zero temperature, the free Fermi gas (FFG) step function is replaced by the momentum distribution $n_{\mathbf{k}}^J$, which includes both the depletion below k_F^J and the HMT:

$$\int_0^{k_F^J} \overbrace{(\text{FFG step function}) f d\mathbf{k}}^{\Theta(k_F^J - |\mathbf{k}|)} \rightarrow \int_0^{\phi_J k_F^J} n_{\mathbf{k}}^J(\text{HMT}) f d\mathbf{k}. \quad (9)$$

In this sense, $n_{\mathbf{k}}^J$ not only modifies the kinetic contribution through the momentum integration, but also effectively incorporates interaction effects, since coefficients such as C_0 inherently reflect nucleon-nucleon interactions [100]. In other words, the modification should be understood in the quasi-nucleon picture.

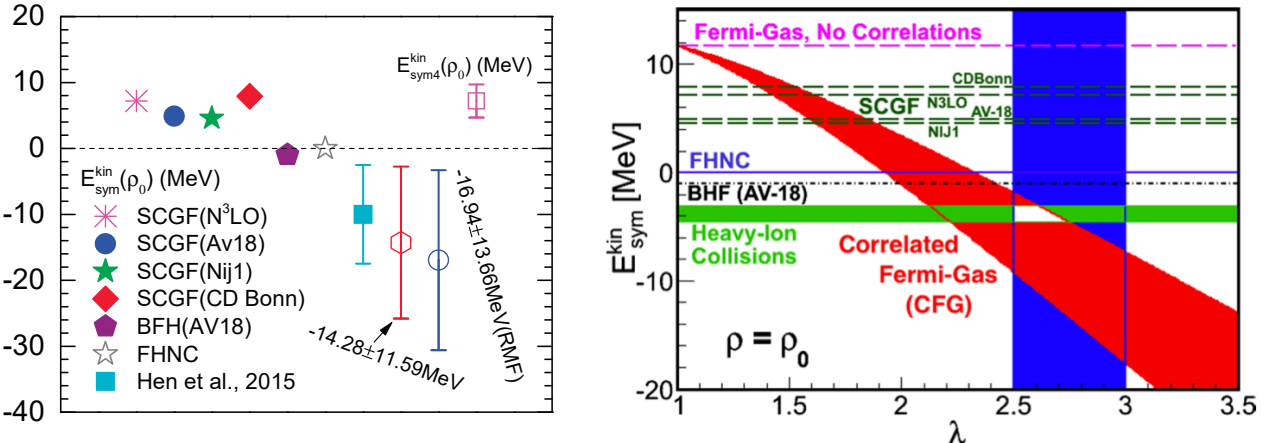


FIG. 5: (Color Online). Left: the kinetic symmetry energy and the isospin-quartic term including the SRC-induced HMT in comparison with predictions by other theories. Figure taken from Ref. [62]. Right: the kinetic symmetry energy using a phenomenological parameterization of Ref. [114]; here the parameter λ is the high-momentum cutoff.

The SRC-induced reduction of the kinetic symmetry energy relative to the FFG prediction is a robust feature observed across many-body theories that include SRC effects. As illustrated in the left panel of FIG. 5, comparisons with microscopic many-body and phenomenological models, including the SCGF prediction (N³LO, AV18, Nij1, CD Bonn) [168], BHF with AV18 plus Urbana IX three-body-force [169], the Fermi hypernetted chain (FHNC) model [170], and phenomenological parametrizations [114], consistently show that SRC reduces the kinetic symmetry energy, although quantitative differences exist. In particular, one finds $E_0^{\text{kin}}(\rho_0) \approx 39.77 \pm 8.13$ MeV for the kinetic EOS of SNM, $E_{\text{sym}}^{\text{kin}}(\rho_0) \approx -14.28 \pm 11.59$ MeV for the kinetic symmetry energy, and a large quartic term $E_{\text{sym},4}^{\text{kin}}(\rho_0) \approx 7.18 \pm 2.52$ MeV [101]. The latter two quantities are displayed in the left panel of FIG. 5. Including relativistic corrections further gives $E_{\text{sym}}^{\text{kin}}(\rho_0) \approx -12.01 \pm 8.23$ MeV [167]. In the right panel of FIG. 5, the kinetic symmetry energy obtained in Ref. [114] is shown, where λ denotes the high-momentum cutoff. In that work, the single-nucleon momentum distribution is parameterized as

$$\bar{n}(\mathbf{k}) = \begin{cases} A, & 0 < |\mathbf{k}| < k_F, \\ C_{\infty}/|\mathbf{k}|^4, & k_F < |\mathbf{k}| < \lambda k_F^0, \end{cases} \quad (10)$$

where C_∞ is the HMT strength, k_F^0 is the Fermi momentum at saturation density ρ_0 , and A is fixed by the normalization condition $[g/(2\pi)^3] \int_0^\infty \bar{n}(\mathbf{k}) d\mathbf{k} = 1$ with $g = 2$ (slightly different from that in Eq. (4)). Using this distribution, one obtains

$$\langle k^j \rangle = \frac{g}{(2\pi)^3} \int_0^\infty k^j \bar{n}(\mathbf{k}) d\mathbf{k} = \frac{3k_F^j}{j+3} - \frac{g c_0 k_F^j}{2\pi^2} \left[\frac{4j}{j^2+2j-3} - \frac{1}{\lambda} \frac{3}{j+3} \left(\frac{\rho}{\rho_0} \right)^{1/3} - \frac{\lambda^{j-1}}{j-1} \left(\frac{\rho_0}{\rho} \right)^{j/3-1/3} \right], \quad (11)$$

where $C_\infty = c_0 k_F$, with $c_0 \sim a_2(\infty)$ taken as a constant [114]. For the special case $j = 2$, and using the parabolic approximation, the kinetic symmetry energy becomes [114]

$$E_{\text{sym}}^{\text{kin}}(\rho) = (2^{2/3} - 1) \cdot \frac{3k_F^2}{10M_N} - \frac{c_0}{\pi^2} \frac{k_F^2}{2M_N} \left[\frac{3}{5} \frac{1}{\lambda} \left(\frac{\rho}{\rho_0} \right)^{1/3} + \lambda \left(\frac{\rho_0}{\rho} \right)^{1/3} - \frac{8}{5} \right], \quad (12)$$

where the HMT in PNM is neglected (an approximation). This analysis yields $E_{\text{sym}}^{\text{kin}}(\rho_0) \approx -10 \pm 7.5 \text{ MeV}$ [114], as shown by the red band in the right panel of FIG. 5. The reduction of the kinetic symmetry energy by SRCs not only impacts our understanding of the origin of symmetry energy but also influences isovector observables [56, 113, 114, 129, 171–183], such as the free neutron/proton and π^-/π^+ ratios in heavy-ion collisions. Furthermore, the potential effects of a large quartic term [101] on heavy-ion collisions have not been explored due to the relatively small isospin asymmetry δ in typical reactions. However, in neutron-rich systems, such as reactions involving rare isotopes or peripheral collisions of heavy nuclei with thick neutron skins and NS environments, the isospin quartic term may play an important role. Typically, the EOS of neutron-rich nucleonic matter is expressed as a sum of a FFG kinetic term and a potential energy truncated at the isospin-quadratic term. Results in Ref. [101] highlight the importance of including the isospin-quartic term in both kinetic and potential contributions. An accurate extraction of the potential isospin-quartic term $E_{\text{sym},4}^{\text{pot}}(\rho)\delta^4$ requires using the kinetic EOS of quasi-particles, which features a reduced symmetry energy and an enhanced quartic term due to the isospin-dependent HMT.

Two complementary approaches have been developed in the literature to incorporate the SRC-HMT-affected potential contribution into the full EOS of ANM. The first adopts an effective nucleon potential model, while the second embeds SRC-induced HMT effects directly into a relativistic field-theoretical framework. As an example of the former, Ref. [184] employs a Gogny-type momentum-dependent potential [185–187], leading to

$$E(\rho, \delta) = E^{\text{kin}}(\rho, \delta) + \frac{A_\ell(\rho_p^2 + \rho_n^2)}{2\rho\rho_0} + \frac{A_u \rho_p \rho_n}{\rho\rho_0} + \frac{B}{\sigma+1} \left(\frac{\rho}{\rho_0} \right)^\sigma (1 - x\delta^2) + \sum_{J,J'} \frac{C_{J,J'}}{\rho\rho_0} \int d\mathbf{k} d\mathbf{k}' f_J(\mathbf{r}, \mathbf{k}) f_{J'}(\mathbf{r}, \mathbf{k}') \Omega(\mathbf{k}, \mathbf{k}'), \quad (13)$$

where $E^{\text{kin}}(\rho, \delta)$ is defined in Eq. (4), Ω is the regulator function and $f_J(\mathbf{r}, \mathbf{k}) = (2/h^3) n_{\mathbf{k}}^J(\rho, \delta)$ is the nucleon phase-space distribution function. In the FFG limit, $f_J(\mathbf{r}, \mathbf{k}) = (1/4\pi^3) \Theta(k_F^J - |\mathbf{k}|)$. The full EOS of SNM and the corresponding kinetic symmetry energy within this framework are summarized in Ref. [184]. A parallel treatment can be carried out within relativistic models. For instance, in the nonlinear Walecka model [58, 100, 188–190],

$$\mathcal{L}_{\text{Walecka}} = \bar{\psi} [\gamma_\mu (i\partial^\mu - g_\omega \omega^\mu - g_\rho \vec{\rho}^\mu \cdot \vec{\tau}) - (M_N - g_\sigma \sigma)] \psi + \frac{1}{2} (\partial_\mu \sigma \partial^\mu \sigma - m_\sigma^2 \sigma^2) - \frac{1}{4} \omega_{\mu\nu} \omega^{\mu\nu} + \frac{1}{2} m_\omega^2 \omega_\mu \omega^\mu - \frac{1}{3} b_\sigma M_N (g_\sigma \sigma)^3 - \frac{1}{4} c_\sigma (g_\sigma \sigma)^4 + \frac{1}{4} c_\omega (g_\omega^2 \omega_\mu \omega^\mu)^2 + \frac{1}{2} m_\rho^2 \vec{\rho}_\mu \cdot \vec{\rho}^\mu - \frac{1}{4} \vec{\rho}_{\mu\nu} \cdot \vec{\rho}^{\mu\nu} + \frac{1}{2} \Lambda_V g_\rho^2 \vec{\rho}_\mu \cdot \vec{\rho}^\mu \Lambda_V g_\omega^2 \omega_\mu \omega^\mu, \quad (14)$$

one obtains the full EOS of SNM, $E_0(\rho) = \varepsilon_0/\rho - M_N$ [100],

$$\begin{aligned} \varepsilon_0(\rho) = & \frac{\Delta_0 M_0^{*,4}}{\pi^2} \left[\frac{1}{4} \theta (1 + \theta^2)^{3/2} - \frac{1}{8} \theta \sqrt{1 + \theta^2} - \frac{1}{8} \text{arcsinh} \theta \right] + \frac{C_0 k_F^4}{\pi^2} \left[V(\theta) - \sqrt{1 + \frac{1}{\phi_0^2 \theta^2}} + \sqrt{1 + \frac{1}{\theta^2}} \right] \\ & + \frac{1}{2} m_\sigma^2 \bar{\sigma}^2 + \frac{1}{3} b_\sigma M_N g_\sigma^3 \bar{\sigma}^3 + \frac{1}{4} c_\sigma g_\sigma^4 \bar{\sigma}^4 + \frac{1}{2} m_\omega^2 \bar{\omega}_0^2 + \frac{3}{4} c_\omega (g_\omega \bar{\omega}_0)^3, \end{aligned} \quad (15)$$

together with the symmetry energy:

$$\begin{aligned} E_{\text{sym}}^{\text{kin}}(\rho) = & \frac{g_\rho^2 \rho}{2Q_\rho} + \frac{k_F^2}{6E_F^*} \left[1 - 3C_0 \left(1 - \frac{1}{\phi_0} \right) \right] - 3E_F^* C_0 \left[C_1 \left(1 - \frac{1}{\phi_0} \right) + \frac{\phi_1}{\phi_0} \right] \\ & - \frac{9M_0^{*,4}}{8k_F^3} \frac{C_0 \phi_1 (C_1 - \phi_1)}{\phi_0} \left[2\theta (1 + \theta^2)^{3/2} - \theta \sqrt{1 + \theta^2} - \text{arcsinh} \theta \right] \end{aligned}$$

$$\begin{aligned}
& + \frac{2k_F C_0 (6C_1 + 1)}{3} \left[V(\theta) - \sqrt{1 + \frac{1}{\phi_0^2 \theta^2}} + \sqrt{1 + \frac{1}{\theta^2}} \right] + \frac{C_0 (4 + 3C_1)}{3} \left[\frac{F_F^* (1 + 3\phi_1)}{\phi_0} - E_F^* \right] \\
& + \frac{3k_F C_0}{2} \left[\frac{(1 + 3\phi_1)^2}{9} \left(\frac{\phi_0 k_F}{F_F^*} - \frac{2F_F^*}{\phi_0 k_F} \right) + \frac{2F_F^* (3\phi_1 - 1)}{9\phi_0 k_F} - \frac{1}{9} \frac{k_F}{E_F^*} + \frac{4E_F^*}{9k_F} \right], \tag{16}
\end{aligned}$$

where $Q_\rho = m_\rho^2 + \Lambda_V g_\omega^2 g_\rho^2 \bar{\omega}_0^2$, $\theta = k_F/M_0^*$ is generally smaller than 1, and $V(\theta) = \text{arcsinh}(\phi_0 \theta) - \text{arcsinh} \theta$. We also define $F_F^* = \sqrt{M_0^{*2} + p_F^2}$ with $p_F = \phi_0 k_F$ [100]. Eq. (16) reduces to the standard RMF expression $E_{\text{sym}}(\rho) = k_F^2/6E_F^* + g_\rho^2 \rho/2Q_\rho$ when $\phi_0 = 1$ and $\phi_1 = 0$ are taken.

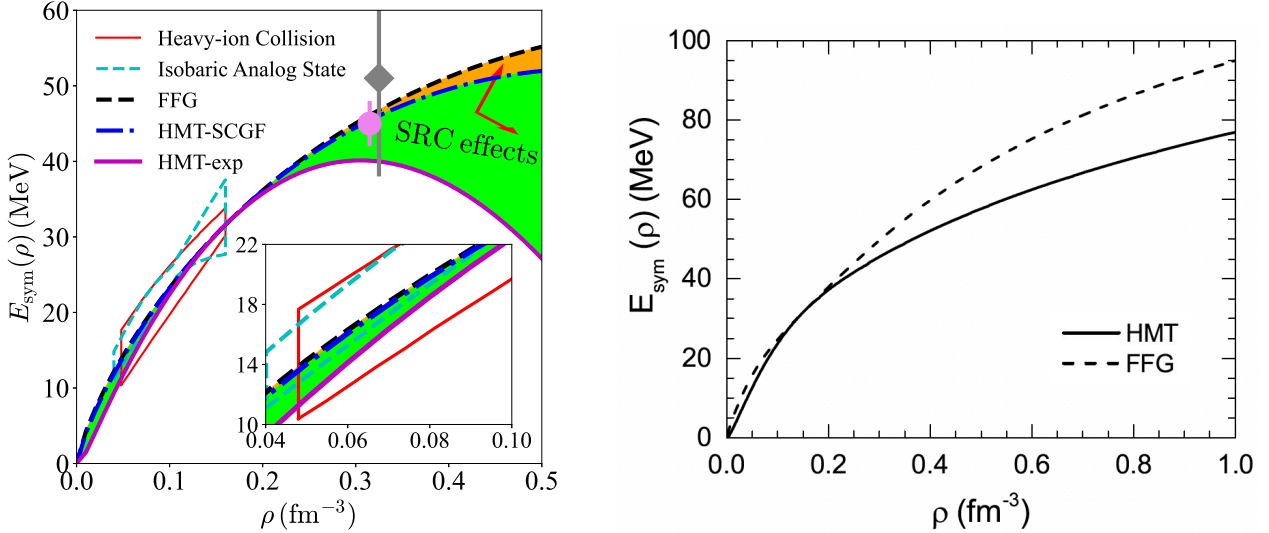


FIG. 6: (Color Online). Left: density dependence of the symmetry energy in the FFG model and HMT model using the Gogny-type momentum-dependent interaction. Constraints from heavy-ion collisions [191] and the isobaric analog state studies [192] are shown; figure taken from Ref. [184]. Right: the same as the left panel but using the nonlinear Walecka model; figure taken from Ref. [103].

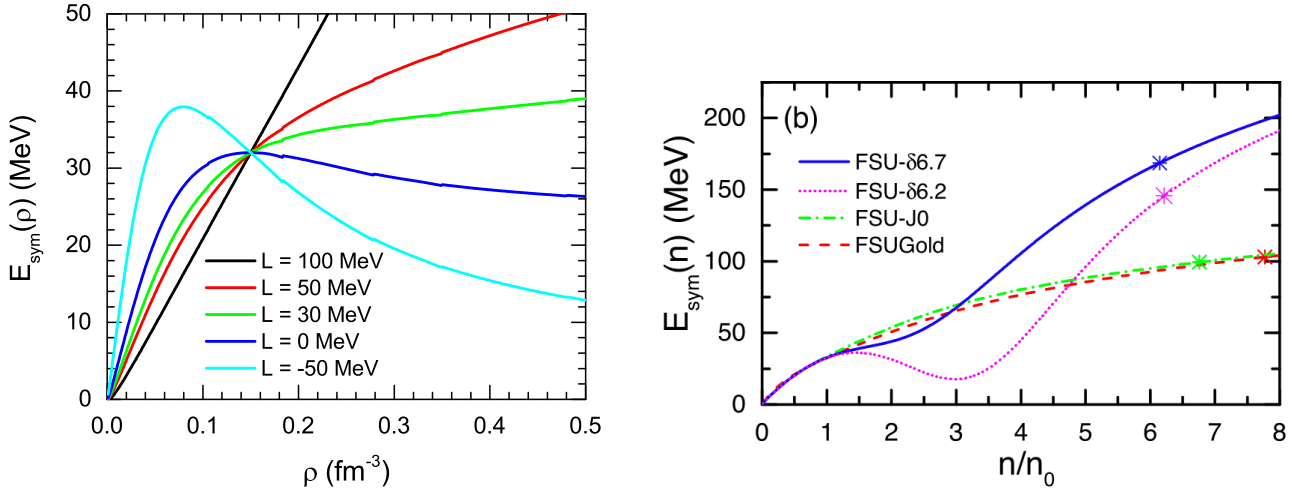


FIG. 7: (Color Online). Left: the symmetry energy with different L as a function of density in the nonlinear Walecka model with SRC-induced HMT, the symmetry energy at the saturation density is fixed; figure adapted from Ref. [62]. Right: the symmetry energy from the nonlinear Walecka model by including the σ - δ coupling; figure taken from Ref. [193].

The inclusion of HMT therefore makes $E_{\text{sym}}^{\text{kin}}(\rho)$ depend solely on the Dirac effective mass $M_0^* \equiv M_N - g_\sigma \bar{\sigma}$, and leads to a consistently reduced kinetic symmetry energy compared with the FFG prediction. At $M_0^*/M_N = 0.6$, for example, one finds $E_{\text{sym}}^{\text{kin}}(\rho_0) \approx -16.94 \pm 13.66 \text{ MeV}$ [103], in close agreement with the corresponding non-relativistic estimates (see the left panel of FIG. 5). This reduction is thus a robust and model-independent feature of incorporating SRC-induced high-momentum correlations. The density dependence of the symmetry energy obtained from both the non-relativistic potential model and the relativistic Walecka framework is displayed in FIG. 6. As seen in the figure, SRC-induced HMT effects reduce the

symmetry energy in both approaches across sub-saturation and supra-saturation densities. In other words, the symmetry energy is softened at high densities while being hardened at low densities. The corresponding SRC-HMT modifications to the symmetric pressure $P_0(\rho)$ are also examined in both models. Although the qualitative trend is consistent, the magnitude of the change in $P_0(\rho)$ is model-dependent. Such variations can affect NS properties, particularly the mass-radius relation. We shall discuss these implications further in Section C.

The softening of the symmetry energy at $\rho \gtrsim \rho_0$ induced by the SRC-HMT effects in the nonlinear Walecka model also allows one to generate a flat, or even bending-down, behavior of $E_{\text{sym}}(\rho)$ at intermediate densities. Such a feature is difficult to achieve in conventional RMF models. In other words, by varying the slope parameter L while keeping $E_{\text{sym}}(\rho_0)$ fixed, it becomes possible to construct a very soft symmetry energy that even decreases at high densities; see the left panel of FIG. 7. There is circumstantial evidence suggesting that a super-soft $E_{\text{sym}}(\rho)$ may be required to reproduce the π^-/π^+ ratio in heavy-ion collisions [194]. Moreover, recent studies incorporating NS astrophysical constraints (e.g., tidal deformabilities) also support this possibility [193, 195–197]. Illustrated in the right panel of FIG. 7 are the symmetry energies obtained in a recent RMF model study [193]; in this work, the RMF model can be made simultaneously consistent with: (1) the EOS of symmetric matter at supra-saturation densities extracted from flow data [14] in heavy-ion collisions; (2) the neutron skin thickness of ^{208}Pb from the PREX-II experiment [198]; (3) the largest observed NS mass, from PSR J0740+6620 [68, 78]; (4) the upper limit $\Lambda_{1.4} \lesssim 580$ on the tidal deformability of a $1.4 M_\odot$ NS from GW170817 [64]; and (5) the M-R radius measurements of PSR J0030+0451 [69, 82] and PSR J0740+6620 by NICER [68, 78]. It effectively resolves the well-known tension between PREX-II and GW170817 present in conventional RMF descriptions; as shown in the figure, achieving such consistency requires a flat symmetry energy roughly around $\rho/\rho_0 \approx 2 \sim 3$, as exemplified by the FSU- δ 6.7 and FSU- δ 6.2 parameter sets. It is also interesting to note here that such a flattened symmetry energy at intermediate densities is closely related to the appearance of a characteristically peaked density profile of the speed of sound in NSs as recently demonstrated quantitatively in Refs. [199, 200].

In short, SRC-induced HMTs impart substantial modifications to the EOS of ANM. Specifically, they stiffen the kinetic EOS of SNM, markedly reduce $E_{\text{sym}}^{\text{kin}}(\rho)$, and enhance $E_{\text{sym},4}^{\text{kin}}(\rho)$. To ensure that the total symmetry energy $E_{\text{sym}}(\rho)$ remains consistent with empirical constraints at ρ_0 , the reduced kinetic contribution necessitates a corresponding adjustment of the potential part, thereby altering the density dependence of both the isoscalar and isovector channels. In practice, the SRC-modified momentum distribution $n_{\mathbf{k}}'$ constitutes the fundamental input for evaluating all kinetic and interaction-related quantities in both non-relativistic and relativistic field frameworks. Across models, the HMT consistently softens $E_{\text{sym}}(\rho)$ at supra-saturation densities ($\rho \gtrsim \rho_0$) while hardening it at sub-saturation densities, also influencing higher-order isospin-dependent terms and momentum-dependent effects. Moreover, recent studies have extended these analyses to general space dimension d [201], leveraging concepts from ultracold atomic physics [39, 40, 202] and theoretical techniques such as the ϵ -expansion from statistical physics [203–205]. These SRC-HMT-induced EOS modifications naturally propagate to the NS structure, as discussed in the following section.

C SRC-HMT Effects on Neutron Star Properties: Selected Results with Open Issues

The SRC-induced HMT, particularly its isospin dependence, is expected to influence the properties of cold NSs, as the neutron-rich environment enhances the proton high-momentum component, thereby amplifying its dynamical impact. The NS mass is determined by integrating the Tolmann–Oppenheimer–Volkoff (TOV) equations (setting $c = 1$) [206, 207]:

$$\frac{dP}{dr} = -\frac{GM\epsilon}{r^2} \left(1 + \frac{P}{\epsilon}\right) \left(1 + \frac{4\pi r^3 P}{M}\right) \left(1 - \frac{2GM}{r}\right)^{-1}, \quad \frac{dM}{dr} = 4\pi r^2 \epsilon, \quad (17)$$

where $M = M(r)$, $P = P(r)$, and $\epsilon = \epsilon(r)$ denote the mass, pressure, and energy density at the radial coordinate r . The equations are highly nonlinear and are solved numerically by choosing a central pressure and integrating outward to the stellar radius R where $P(R) = 0$ for a given EOS $P(\epsilon)$. The resulting gravitational mass is $M_{\text{NS}} \equiv M(R) = \int_0^R 4\pi r^2 \epsilon(r) dr$.

The left panel of FIG. 8 illustrates the construction of the β -equilibrium EOS employed in NS calculations. For neutrino-free β -stable nuclear matter, chemical equilibrium for the processes $\text{n} \rightarrow \text{p} + \text{e}^- + \bar{\nu}_e$ and $\text{p} + \text{e}^- \rightarrow \text{n} + \nu_e$ requires $\mu_e = \mu_n - \mu_p \approx 4\delta E_{\text{sym}}(\rho) + 8\delta^3 E_{\text{sym},4}(\rho)$, where μ_i ($i = \text{n}, \text{p}, \text{e}, \mu$) denotes the corresponding chemical potential. For relativistic degenerate electrons, one has $\mu_e = (m_e^2 + k_F^{e,2})^{1/2} = [m_e^2 + (3\pi^2 \rho x_e)^{2/3}]^{1/2} \approx (3\pi^2 \rho x_e)^{1/3}$, where $m_e \approx 0.511 \text{ MeV}$ is the electron mass and charge neutrality imposes $x_p = x_e$. Once the electron chemical potential exceeds the muon rest mass $m_\mu \approx 0.105 \text{ GeV}$, the reactions $\text{e}^- \rightarrow \mu^- + \nu_e + \bar{\nu}_\mu$, $\text{p} + \mu^- \rightarrow \text{n} + \nu_\mu$, and $\text{n} \rightarrow \text{p} + \mu^- + \bar{\nu}_\mu$ become energetically allowed. The appearance of muons modifies the β -equilibrium conditions to $\mu_n - \mu_p = \mu_e$ and $\mu_n - \mu_p = \mu_\mu = [m_\mu^2 + (3\pi^2 \rho x_\mu)^{2/3}]^{1/2}$, with $x_p = x_e + x_\mu$. For npe μ matter, the total energy density is $\epsilon(\rho, \delta) = \epsilon_{\text{N}}(\rho, \delta) + \epsilon_{\text{e}}(\rho, \delta) + \epsilon_{\mu}(\rho, \delta)$, where the nucleonic

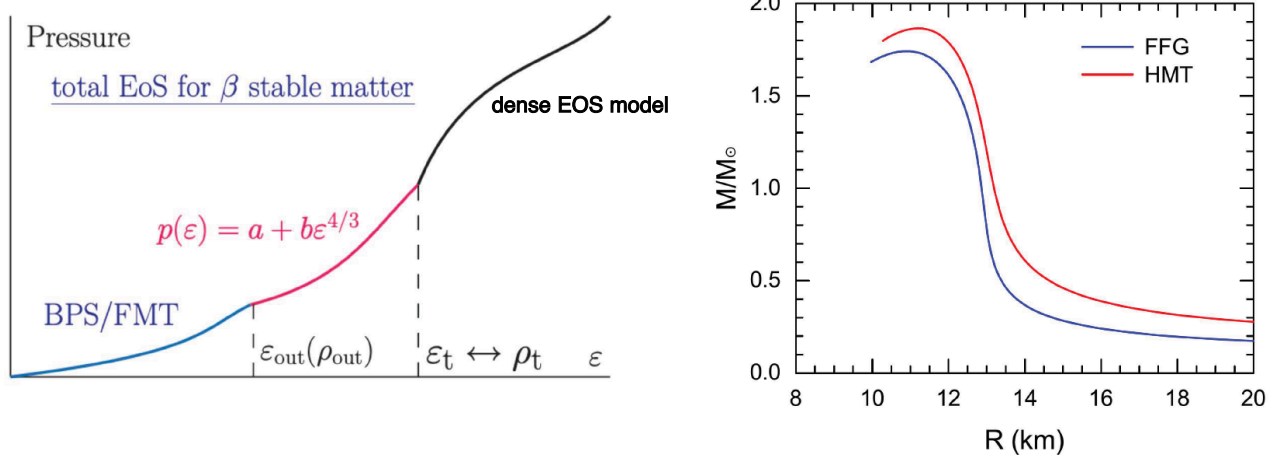


FIG. 8: (Color Online). Left: construction of β -stable EOS in NS calculations. Right: the NS M-R relation obtained by integrating the TOV equation under the EOS of NS matter in the FFG and HMT models, respectively. Figure taken from Ref. [100].

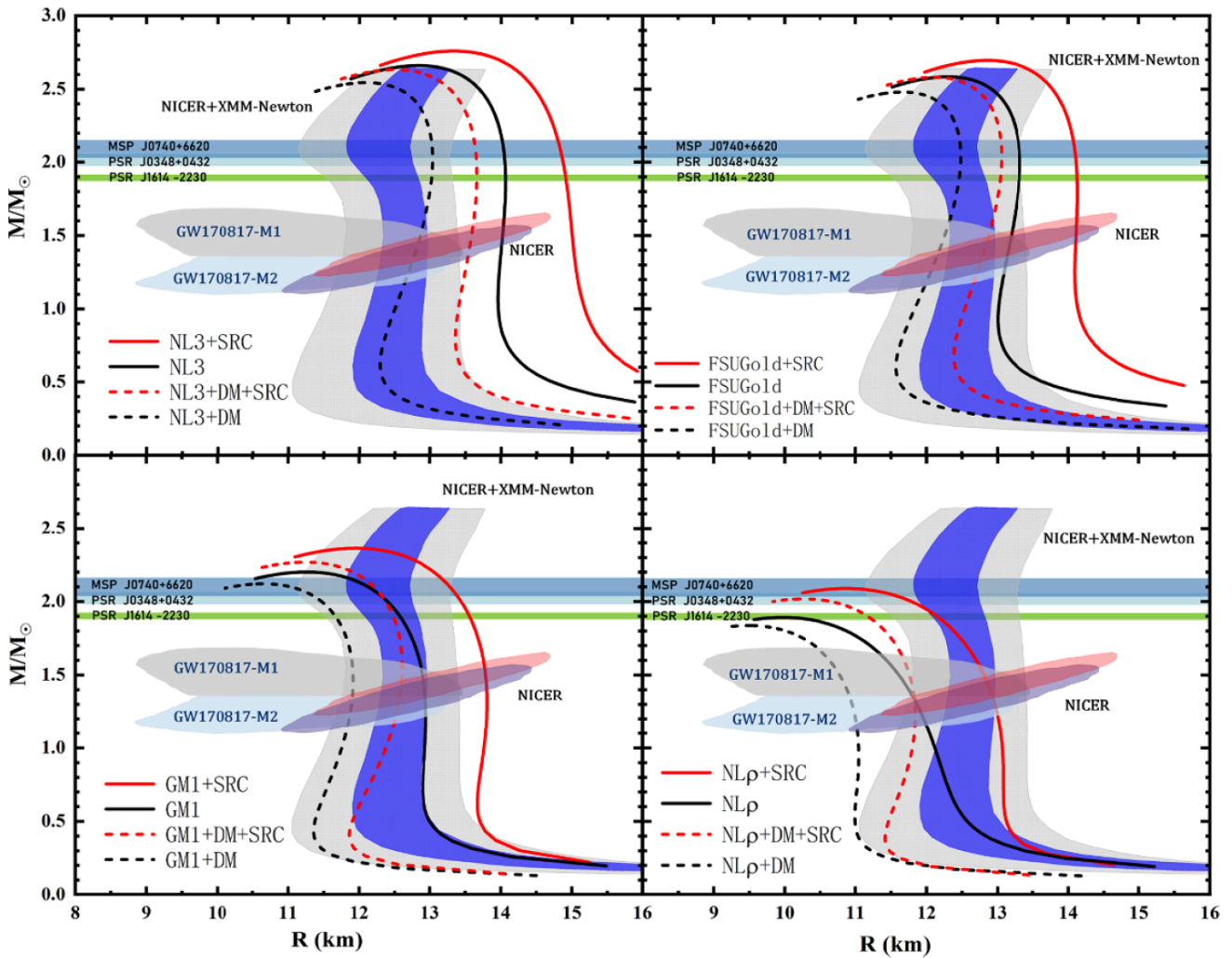


FIG. 9: (Color Online). NS M-R relations calculated using four widely employed relativistic parameter sets, each shown in four variants: the original version (black solid), the SRC-revised version (red solid), the dark-matter (DM) revised version (black dashed), and the SRC+DM revised version (red dashed). Figure taken from Ref. [208].

contribution is that of np matter, $\varepsilon_N(\rho, \delta) = [M_N + E(\rho, \delta)]\rho$, with $E(\rho, \delta)$ the EOS of ANM. The leptonic energy densities

are computed in the FFG approximation, $\varepsilon_\ell(\rho, \delta) = \eta_\ell \phi_\ell(t_\ell)$, with $\eta_\ell = m_\ell/8\pi^2\lambda_\ell^3$, $\lambda_\ell = m_\ell^{-1}$, $t_\ell = \lambda_\ell(3\pi^2\rho_\ell)^{1/3}$, and

$$\phi_\ell(t_\ell) = t_\ell(1+2t_\ell^2)\sqrt{1+t_\ell^2} - \ln(t_\ell + \sqrt{1+t_\ell^2}), \quad (18)$$

where m_ℓ and ρ_ℓ denote the lepton masses and number densities. The total pressure is then $P(\rho, \delta) = P_N(\rho, \delta) + P_e(\rho, \delta) + P_\mu(\rho, \delta)$, with the nucleonic pressure given by the Hugenholtz–Van Hove (H VH) theorem [209–211], $P_N(\rho, \delta) = \rho_p \mu_p + \rho_n \mu_n - \varepsilon_N(\rho, \delta)$. The leptonic contributions satisfy $P_\ell(\rho, \delta) = \rho_\ell \mu_\ell - \varepsilon_\ell(\rho, \delta)$, where $\mu_\ell = \sqrt{k_\ell^2 + m_\ell^2}$ and $k_\ell = (3\pi^2\rho_\ell)^{1/3}$. Within this formalism, the H VH relation, $P = \rho^2 d(\varepsilon/\rho)/d\rho$ is automatically fulfilled. The transition density ρ_t denotes the baryon number density separating the liquid core from the inner crust in NSs [212]. A simple and widely adopted approach for determining ρ_t is the thermodynamical method, which requires the system to satisfy the intrinsic stability conditions

$$-\left(\frac{\partial P}{\partial v}\right)_{\mu_{\text{np}}} > 0, \quad -\left(\frac{\partial \mu_{\text{np}}}{\partial q_c}\right)_v > 0, \quad (19)$$

where P is the total pressure, v and q_c denote the volume and charge per baryon, and $\mu_{\text{np}} = \mu_n - \mu_p$ is the neutron-proton chemical potential difference. Using the relations $\partial E(\rho, x_p)/\partial x_p = -\mu_{\text{np}}$ and $x_p = \rho_p/\rho$, and treating the electrons as a free Fermi gas, one finds that the thermodynamical stability criteria in Eq. (19) are equivalent to requiring the incompressibility of NS matter at β -equilibrium to stay positive [212–214]

$$K_\mu(\rho) = 2\rho \frac{\partial E(\rho, x_p)}{\partial \rho} + \rho^2 \frac{\partial^2 E(\rho, x_p)}{\partial \rho^2} - \left(\frac{\partial^2 E(\rho, x_p)}{\partial \rho \partial x_p} \rho \right)^2 \left| \frac{\partial^2 E(\rho, x_p)}{\partial x_p^2} \right| > 0. \quad (20)$$

The baryon number density at which Eq. (20) is first violated then defines the core-crust transition density ρ_t ; consequently $P_t = P(\rho_t)$. Moreover, near the very surface of the NS, the EOS is often taken as the BPS/FMT form [215, 216]. As the density increases, one encounters the outer crust and eventually reaches the core-crust interface, the ρ_t of which is obtained self-consistently within the employed model. For the EOS between the outer crust and the transition boundary, a frequently used parametrization is

$$P(\varepsilon) = a + b \varepsilon^{4/3}, \quad (21)$$

where the coefficients a and b are determined consistently with the calculated transition density. The outer-crust density is taken to be $\rho_{\text{out}} \approx 2.46 \times 10^{-4} \text{ fm}^{-3}$. In the region $6.93 \times 10^{-13} \text{ fm}^{-3} \lesssim \rho \lesssim \rho_{\text{out}}$, the BPS EOS is employed, while for $4.73 \times 10^{-15} \text{ fm}^{-3} \lesssim \rho \lesssim 6.93 \times 10^{-13} \text{ fm}^{-3}$ the FMT EOS is used [215, 216].

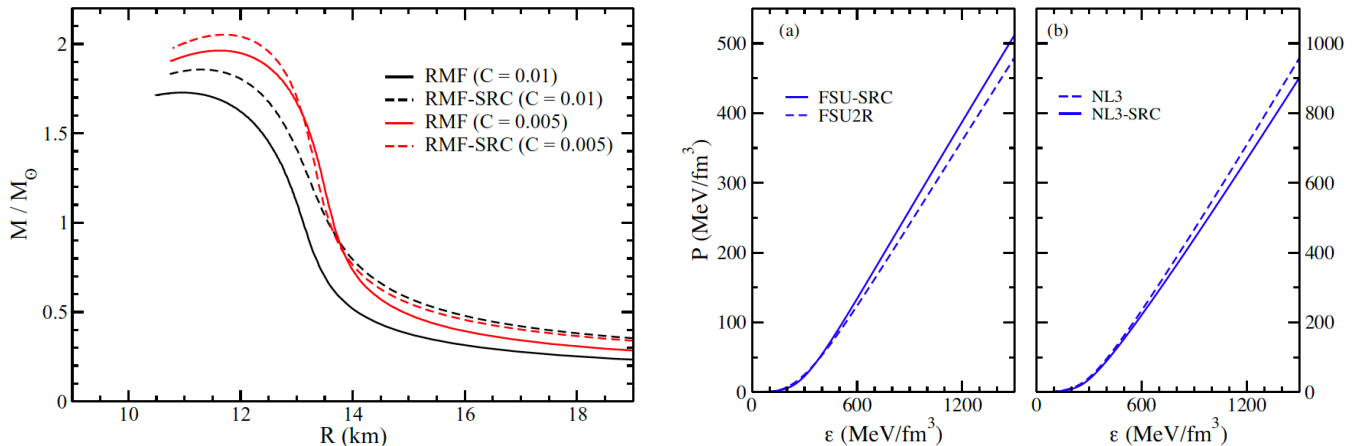


FIG. 10: (Color Online). Left: the NS M-R relations in the nonlinear Walecka model with and without SRC-HMT effects. Here, C denotes the strength of the ω -meson self-interaction term, $\sim C(\omega_\mu \omega^\mu)^2$; figure adapted from Ref. [217]. Right: similar to the left panel, but for two parameter sets: one including the ω -meson self-interaction term (FSU-2R) [218] and one without (NL3) [219]; figure adapted from Ref. [220].

SRC-induced HMT effects influence various NS properties, such as the M-R relation and tidal deformabilities, in several ways: (a) they modify the proton fraction x_p , which directly affects the composition of NS matter and plays a crucial role in determining the NS cooling behavior [85, 86, 221–223]; and (b) they also reshape the dense-matter EOS at supra-saturation densities, as discussed in the previous section. Together, these effects can impact the NS mass and radius [208, 224–226], tidal deformabilities [217, 227, 228], oscillation spectra [208, 229], and other macroscopic observables. Shown in the right

panel of FIG. 8 is the predicted NS M-R relation obtained using the FFG and HMT models within the nonlinear Walecka framework [100]. Although the symmetry energy is softened at high densities, the EOS of SNM is substantially stiffened, leading to an overall enhancement of the maximum NS mass. In particular, the SRC-HMT increases the skewness parameter J_0 of the SNM EOS [100], which plays a crucial role in determining NS masses [230]. In contrast, the impact of the symmetry energy on the M-R relation is comparatively weak in RMF models [188]. As a result, the increased skewness induced by the HMT elevates the maximum NS mass. Quantitatively, the maximum masses for the HMT and FFG cases are $M_{\text{NS}}^{\text{max}} \approx 1.87 M_{\odot}$ and $M_{\text{NS}}^{\text{max}} \approx 1.74 M_{\odot}$, with corresponding radii of approximately 11.21 km and 10.89 km [100], respectively. This represents an $\sim 8\%$ increase in $M_{\text{NS}}^{\text{max}}$. While the HMT EOS still underpredicts the observed maximum masses, it moves the theoretical predictions closer to current astrophysical measurements [68–70, 77–84].

After the work of Ref. [100], several related studies have been conducted [208, 217, 220, 224, 225, 227–229, 231]. For instance, Ref. [224] employed the same nonlinear Walecka model to examine the NS cooling pattern with and without SRC-HMT effects, and also analyzed the NS M-R relation. Similarly, Ref. [208] adopted a slightly modified parametrization of $n(k)$ in the nonlinear Walecka model, with and without dark-matter (DM) effects, and the resulting M-R relations are shown in FIG. 9; an enhanced NS maximum mass due to the SRC-HMT is observed. The same conclusion was reported in Ref. [217], as illustrated in the left panel of FIG. 10. Subsequently, the role of the ω -meson self-interaction term, $\sim C(\omega_\mu \omega^\mu)^2 \sim c_\omega (\omega_\mu \omega^\mu)^2$ (see Eq. (14)), was investigated in detail. For example, Ref. [220] found that including this self-interaction term leads the SRC-HMT to enhance the maximum mass (as shown in the left panel of FIG. 10), whereas in its absence the SRC-HMT tends to reduce the maximum mass, see the right panel of FIG. 10 where two parameter sets are constructed: one including the ω -meson self-interaction term (FSU-2R) [218] and one without (NL3) [219]. Thus, there is no definitive evidence as to whether SRC-HMT universally increases or decreases $M_{\text{NS}}^{\text{max}}$. A similar trend was observed in the modified Gogny-type model with a momentum-dependent potential [184], where incorporating SRC-HMT effectively reduces $M_{\text{NS}}^{\text{max}}$. More related works on NSs with DM effects can be found in Refs. [232–246]. Furthermore, Ref. [247] emphasized that although NS observables are sensitive to the high-density behavior of the symmetry energy, they do not provide sufficient discriminatory power to distinguish between HMT and FFG descriptions of the kinetic contribution. Their analysis suggests that the NS EOS inferred from Bayesian analyses of NS observations is robust and largely insensitive to the specific microscopic modeling of $E_{\text{sym}}^{\text{kin}}$. Such insensitivity, or the “blindness” of the TOV equations, is consistent with recent findings based on a dimensionless reformulation of the TOV equations [37].

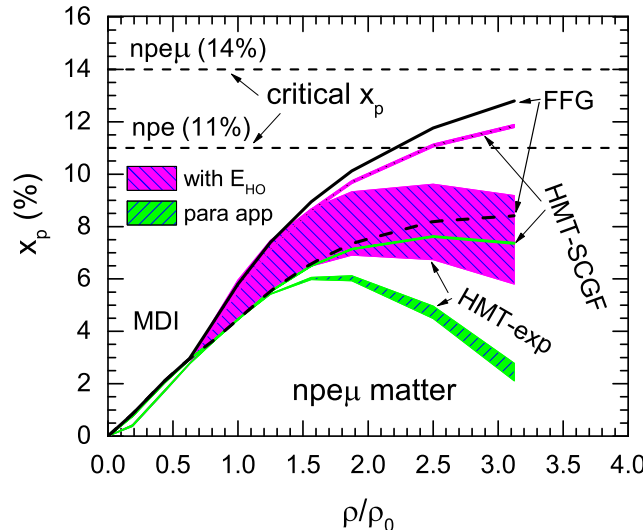


FIG. 11: (Color Online). Proton fraction x_p obtained in the modified Gogny-type model with/without the SRC-induced HMT. The shadow regions are caused by the uncertainties of the macroscopic quantities of the ANM EOS.

As discussed above, the SRC-induced HMT can significantly influence the proton fraction x_p , which is crucial for determining the NS cooling pattern [85, 98]. In the simplest approximation, x_p can be estimated from the symmetry energy as

$$x_p \approx \frac{1}{2} \left[3 + \left(\frac{k_F}{4E_{\text{sym}}(\rho)} \right)^3 \right]. \quad (22)$$

This expression indicates that at very low densities, $k_F/4E_{\text{sym}}(\rho) \rightarrow 3M_N/2k_F \sim \rho^{-1/3}$, so that $x_p \sim \rho$ in this limit. In the

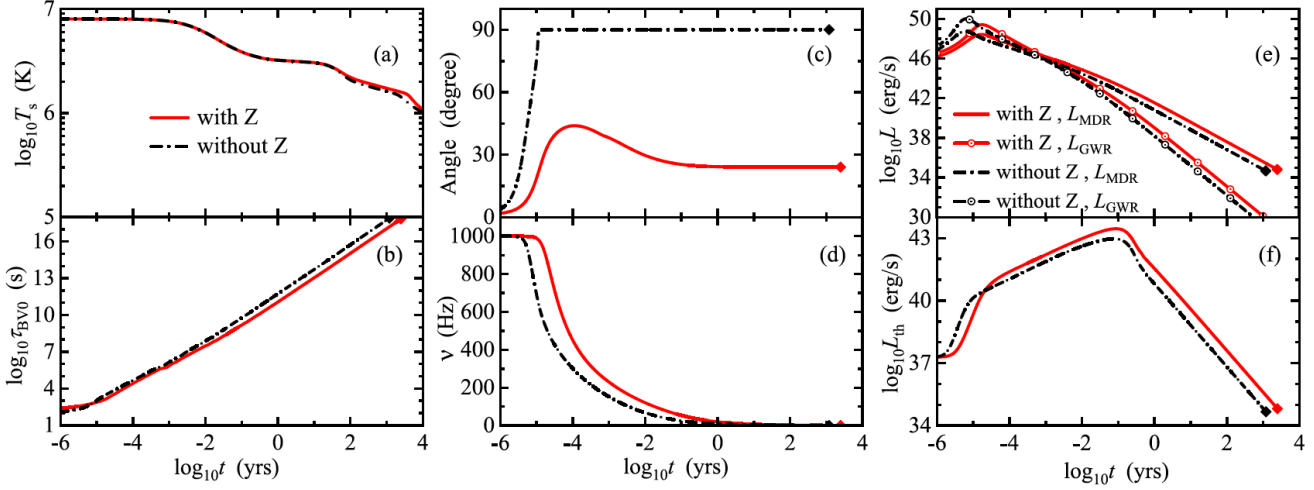


FIG. 12: (Color Online). Impact of the Migdal–Luttinger Z -factor on the evolution of a canonical magnetar ($1.4 M_{\odot}$, $P_0 = 1$ ms), showing its effects on surface temperature T_s , spin frequency ν , magnetic inclination χ , damping timescale τ_{BV0} , and luminosities L_{GW} , L_{MDR} , and L_{th} ; the diamond marks when T reaches the superfluid critical temperature T_c . Figure taken from Ref. [223].

high-density limit, for instance, in the nonlinear Walecka model (of (14)) using a FFG description, the symmetry energy leads to

$$x_p \rightarrow \frac{1}{2} \left/ \left[3 + \left[\left(\frac{3\pi^2}{2} \right)^{1/3} \left/ \left[\frac{2}{3} \left(\frac{3\pi^2}{2} \right)^{1/3} + \frac{2c_{\omega}^{2/3}}{\Lambda_V} \right] \right] \right]^3 \right], \quad (23)$$

with a typical value around 10%, depending on the magnitudes of c_{ω} and Λ_V [167], e.g., $x_p \rightarrow 4/51 \approx 7.8\%$ if $c_{\omega} = 0$, or $x_p \approx 15\%$ for $c_{\omega}^{2/3}/\Lambda_V \approx 1$; $x_p \lesssim 1/6 \approx 16\%$ can be obtained for $c_{\omega}^{2/3}/\Lambda_V \rightarrow \infty$. Due to the complexities of higher-order terms in the EOS of ANM when the HMT is included, we approximate these contributions when determining the x_p as $8E_{\text{sym},4}(\rho)\delta^3 + \dots \approx 8E_{\text{HO}}(\rho)\delta^3$ with $E_{\text{HO}}(\rho) = E_{\text{sym},4}(\rho) + E_{\text{sym},6}(\rho) + \dots = E_n(\rho) - E_0(\rho) - E_{\text{sym}}(\rho)$, where $E_n(\rho)$ is the EOS of PNM. As shown in Ref. [58], including the fourth-order symmetry energy yields x_p values very close to the exact result. This scheme is partly necessitated by the difficulty that the chemical potential is not generally given by $k_F^{n/p,2}/2M_N + U_{n/p}(\rho, \delta, k_F^{n/p})$ once the HMT in $n_{\mathbf{k}}^J$ is considered [248]. FIG. 11 displays the density dependence of the proton fraction x_p in β -stable npe μ matter, obtained within the modified Gogny-type model with and without SRC-HMT effects. The shaded regions account for uncertainties in macroscopic quantities such as K_0 and L . Three main observations can be made: (a) Including the SRC-HMT softens the symmetry energy at supra-saturation densities and reduces x_p at fixed densities relative to the FFG prediction (black line vs. thin magenta and green bands); (b) as the fraction of high-momentum nucleons in finite nuclei and nuclear matter increases, e.g., from the HMT-SCGF set to the HMT-exp set [103], the supra-normal density symmetry energy becomes softer and the corresponding x_p is further reduced; (c) the fourth-order symmetry energy significantly affects x_p ; e.g., in the HMT-exp set it increases x_p at $\rho = 3\rho_0$ from approximately 3.5% to 7.5%.

Notably, within the HMT-exp set [103], the maximum proton fraction x_p never surpasses the threshold for the direct Urca (DU) process, i.e., $\sim 11\%$ for npe matter and $\sim 14\%$ for npe μ matter. This naturally raises the question of whether the DU process is ultimately favorable, considering the SRC-HMT effects. Addressing this issue is highly nontrivial for at least two reasons: (a) The HMT above the Fermi surface may effectively open additional channels for the DU process, potentially lowering the effective proton fraction threshold below the nominal 11% or 14% values [62, 98]; (b) Conversely, the combined effect of the HMT and the low-momentum depletion of $n(k)$ significantly reduces the Migdal–Luttinger jump Z_F^J at the Fermi surface, which in turn strongly affects the neutrino emissivities [86, 221]. Therefore, a rigorous analysis of NS cooling that includes SRC-HMT effects is inherently complex and typically requires more sophisticated treatments, such as those based on the spectral function approach [87]. As an illustration, FIG. 12 displays the influence of the Migdal–Luttinger Z -factor on various evolutionary properties of a canonical magnetar with mass about $1.4 M_{\odot}$; the figure shows that the Z -factor significantly affects some quantities, such as the magnetic inclination angle, while having minimal impact on others. There are numerous intriguing aspects of NS cooling, including the existence/disappearance of the crustal phase structures [249], mean free path calculations [250, 251], and other transport properties such as thermal and electrical conductivities and viscosities [252–259]. We do not attempt a detailed review of these issues here and refer interested readers to Ref. [99] and the references therein.

In short, the SRC-induced HMT, especially its isospin dependence, significantly impacts cold NSs by modifying the pro-

ton fraction x_p and reshaping the dense-matter EOS at supra-saturation densities, which in turn affects the NS M-R relation, tidal deformabilities, oscillation modes, and other macroscopic observables. While the HMT can increase $M_{\text{NS}}^{\text{max}}$ by stiffening the SNM EOS, its effect is strongly model-dependent and intertwined with factors like the ω -meson self-interaction and the Migdal-Luttinger Z -factor, making its influence on the DU process highly nontrivial. Moreover, NS cooling and transport properties, including crustal phases, mean free paths, and viscosities, further complicate the analysis, highlighting the need for detailed studies such as those based on the spectral function approach. In the following, we highlight a few open issues to stimulate further studies on SRC-HMT effects and their impact on certain NS properties.

(1) What is the High-momentum Nucleon Fraction at NS Densities?

Up to now, all information about the nucleon SRC-induced HMT is constrained only at densities $\rho \lesssim \rho_0$, either from experimental analyses [46, 47] or from microscopic many-body calculations [48, 149, 260, 261]. However, when studying NSs, these constraints are implicitly extrapolated to much higher densities. For a typical NS, its central density $\rho_c \approx 5\rho_0$ corresponds to a characteristic Fermi momentum $5^{1/3}k_F(\rho_0) \approx 450$ MeV, which lies well within the momentum range dominated by SRCs, so SRC is relevant near NS centers. A natural question then arises: how reliable is this extrapolation? For instance, in finite nuclei or nuclear matter near saturation density, the high-momentum nucleon fractions exhibit a clear isospin dependence for neutrons and protons, as shown in the right panel of FIG. 4 and sketched by the solid lines in FIG. 13. Yet at supranuclear densities, there is no *a priori* reason to expect $x_J^{\text{HMT}}(\delta)$ to follow the same or even a similar trend; alternative behaviors, such as those suggested by the dashed lines in FIG. 13, are also plausible. Because the δ -dependence of x_J^{HMT} directly affects the kinetic contributions, the symmetry energy, and the composition of dense matter, uncertainties in its high-density behavior can have significant consequences for predictions of NS properties.

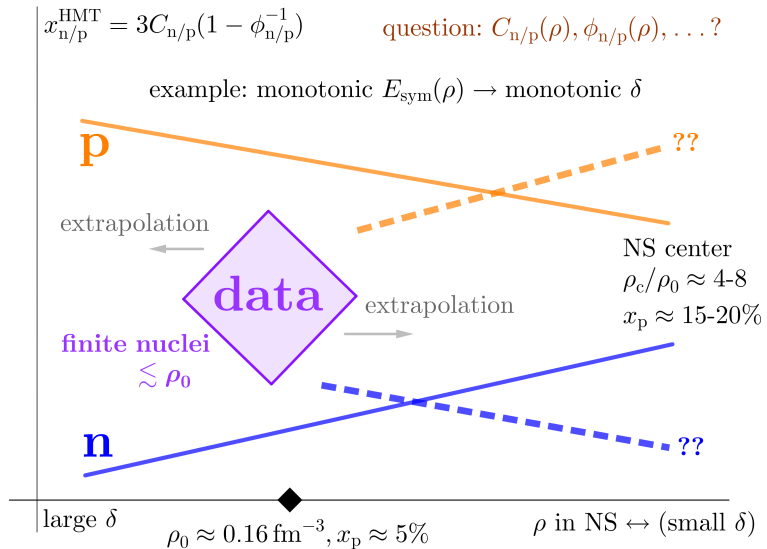


FIG. 13: (Color Online). A sketch of high-momentum fractions of nucleons as functions of nucleon density. Does the high-momentum nucleon fraction at NS densities exhibit a δ -dependence similar to that observed near saturation density? Available data currently only constrain the behavior at $\rho \lesssim \rho_0 \approx 0.16 \text{ fm}^{-3}$. In this sketch, we assume that the symmetry energy $E_{\text{sym}}(\rho)$ increases monotonically with density. Considering two connected regions with local densities ρ_1 and ρ_2 , respectively, the isospin-equilibrium requires that [262] $E_{\text{sym}}(\rho_1)\delta(\rho_1) = E_{\text{sym}}(\rho_2)\delta(\rho_2)$. Consequently, the isospin asymmetry δ in the inner core of a NS is smaller than that near its surface.

Put it in other words, the HMT-related parameters, such as the contact $C_{n/p}$ and the high-momentum cutoff $\phi_{n/p}$, are also expected to depend on the density, namely $C_{n/p} \rightarrow C_{n/p}(\rho)$, $\phi_{n/p} \rightarrow \phi_{n/p}(\rho)$. In this case, the high-momentum fraction x_J^{HMT} may exhibit a nontrivial δ -dependence at different densities. To better constrain the HMT parameters at supra-saturation densities, one may develop more advanced theoretical approaches or propose direct experimental probes, e.g., through heavy-ion collision processes [191, 194, 263–265]. In Ref. [266], the momentum distributions at densities beyond the saturation are studied within an extended Brueckner–Hartree–Fock (eBHF) approach, which may provide useful information on $C_{n/p}$ at these densities. With improved constraints, one could systematically investigate SRC-HMT effects on NS properties by combining: (a) their impact on the EOS of ANM, particularly the symmetry energy, and (b) their influence on the δ -dependence of the HMT parameters. These two aspects are clearly intertwined, since $E_{\text{sym}}(\rho)$ directly determines the proton fraction in NSs, and their coupling may lead to nontrivial implications for NS physics.

(2) Can the SRC-HMT Affect the Inner-crust EOS Index γ of $P = a + b\epsilon^\gamma$?

The EOS of the inner crust, spanning the region between the outer crust and the core-crust transition density ρ_t , is often parametrized using Eq. (21), i.e., $P \approx a + b\epsilon^{4/3}$ [267]. Since the core-crust transition density, $\rho_t \approx 2\rho_0/3$, lies within the density range where SRCs are significant [46], it is natural to expect that SRCs may also affect the inner crust EOS. In particular, an interesting question is whether the index γ in $P \approx a + b\epsilon^\gamma$ could be modified by SRC-HMT effects. To date, dedicated studies exploring this possibility remain scarce.

The inner crust EOS is further intertwined with exotic nuclear structures, including pasta phases [268–270], cluster formation [271–276], and other effective low-dimensional configurations [277–280]. Its properties are also sensitive to the symmetry energy of dilute nuclear matter [281]. While the inner crust EOS may have a limited influence on the mass and radius of massive NSs, it can significantly affect the radius of low-mass NSs. Moreover, it plays an important role in NS cooling and neutrino emission processes, since an enhanced symmetry energy due to cluster correlations [281] would increase the proton fraction x_p , thereby modifying related processes [282, 283].

Overall, these considerations suggest that a more systematic study of SRC effects on the inner crust EOS, including their interplay with cluster formation, pasta phases, and the density dependence of the symmetry energy, could provide valuable insights into NS structure, thermal evolution, and neutrino dynamics [85, 282–284].

(3) Does the SRC-HMT Enhance or Reduce the Maximum NS Mass?

We have discussed that the SRC-HMT may either enhance or reduce the maximum NS mass, depending on the model or the specific nucleon-nucleon interaction employed. Specifically, the effect is sensitive to whether the ω -meson self-interaction term $\sim c_\omega(\omega_\mu\omega^\mu)^2$ is included [217, 227, 228]; similarly, in a Gogny-type model with momentum-dependent interactions, the SRC-HMT has been shown to reduce the maximum mass [184]. Moreover, modifying the fitting scheme of the model can change the quantitative impact of SRC-HMT on NS mass [226]. This naturally raises the question: what is the underlying physical mechanism by which SRC-HMT influences the maximum NS mass?

Some clues emerge from previous studies. It is well known that the effect of the symmetry energy on the maximum NS mass is relatively smaller than that of the symmetric part of the EOS [285]. In Ref. [100], we found that the SRC-HMT induces a larger modification in the EOS of SNM than in the symmetry energy; as a result, the stiffening of the SNM EOS dominates over the softening of the symmetry energy, leading to an increase in the maximum NS mass. In contrast, non-relativistic Gogny-type calculations show that the SRC-HMT has little impact on the SNM EOS, while its effect on the symmetry energy is significant (left panel of FIG. 6). Another relevant factor is the manner in which nuclear parameters are fixed. In our studies, the saturation-density parameters are fixed to empirical values: specifically, the SNM EOS is constrained up to order J_0 , and the symmetry energy up to its slope L , before examining the impact of SRC-HMT on higher-order terms, such as the curvature coefficient $K_{\text{sym}} \equiv 9\rho_0^2 d^2 E_{\text{sym}}(\rho)/d\rho^2|_{\rho_0}$ of nuclear symmetry energy. It is therefore natural that if higher-order nuclear coefficients are also fixed, the SRC-HMT may eventually produce little impact, as the EOSs with and without SRC-HMT would behave similarly up to densities relevant for NS cores.

Overall, systematic investigations along this line are essential to clarify the intrinsic physical mechanisms by which SRC-HMT affects NS mass, radius, and related observables such as tidal deformabilities. Future studies could explore (i) the interplay between SRC-HMT and higher-order EOS parameters, (ii) model-independent constraints on SRC-HMT effects using ab initio calculations or Bayesian analyses of NS observations, and (iii) the combined impact of SRC-HMT on both the SNM EOS and the symmetry energy at supra-saturation densities. Such efforts would provide a more comprehensive understanding of the role of SRCs in dense nuclear matter and their astrophysical implications.

(4) How Does the SRC-HMT Affect the Formation of Exotics?

Exotic particles, such as hyperons and Δ resonances, are expected to appear in NS cores; SRC-HMT is expected to influence their formation patterns. In this context, for example, both the kinetic and potential components of the symmetry energy have been found to separately influence the formation densities of the $\Delta(1232)$ states [286], using the nonlinear RMF models with a FFG $n(k)$. Specifically, for the reactions $\Delta^{++} + n \rightarrow p + p$, $\Delta^+ + n \rightarrow n + p$, $\Delta^0 + p \rightarrow p + n$, and $\Delta^- + p \rightarrow n + n$, the critical densities for Δ formation are determined by [286]:

$$\rho_{\Delta^-}^{\text{crit}} : k_F^{\text{n},2}/2M_0^* \approx \Phi_\Delta + g_{\sigma N}(1-x_\sigma)\bar{\sigma} - g_{\omega N}(1-x_\omega)\bar{\omega}_0 - \left[6(1-x_\rho)E_{\text{sym}}^{\text{pot}}(\rho) + 4E_{\text{sym}}^{\text{kin}}(\rho)\right]\delta, \quad (24)$$

$$\rho_{\Delta^0}^{\text{crit}} : k_F^{\text{n},2}/2M_0^* \approx \Phi_\Delta + g_{\sigma N}(1-x_\sigma)\bar{\sigma} - g_{\omega N}(1-x_\omega)\bar{\omega}_0 - 2(1-x_\rho)E_{\text{sym}}^{\text{pot}}(\rho)\delta, \quad (25)$$

$$\rho_{\Delta^+}^{\text{crit}} : k_F^{\text{p},2}/2M_0^* \approx \Phi_\Delta + g_{\sigma N}(1-x_\sigma)\bar{\sigma} - g_{\omega N}(1-x_\omega)\bar{\omega}_0 + 2(1-x_\rho)E_{\text{sym}}^{\text{pot}}(\rho)\delta, \quad (26)$$

$$\rho_{\Delta^{++}}^{\text{crit}} : k_F^{\text{p},2}/2M_0^* \approx \Phi_{\Delta} + g_{\sigma N}(1-x_{\sigma})\bar{\sigma} - g_{\omega N}(1-x_{\omega})\bar{\omega}_0 + [6(1-x_{\rho})E_{\text{sym}}^{\text{pot}}(\rho) + 4E_{\text{sym}}^{\text{kin}}(\rho)]\delta, \quad (27)$$

where $\Phi_{\Delta} \approx 293$ MeV is the mass difference between the $\Delta(1232)$ and the nucleon, M_0^* is the Dirac nucleon effective mass in SNM, $g_{\sigma N}$ and $g_{\omega N}$ are the meson-nucleon coupling constants, and $x_{\sigma}, x_{\omega}, x_{\rho}$ characterize the Δ -meson couplings. These relations are obtained within a nonlinear RMF framework that explicitly includes Δ -meson interactions. This formalism enables a clear separation of the contributions from the kinetic and potential parts of the symmetry energy to the determination of $\rho_{\Delta}^{\text{crit}}$. In particular, SRCs have been suggested to induce a negative kinetic contribution to the symmetry energy already at normal nuclear density (left panel of FIG. 5). Under such conditions, the relative appearance densities of the Δ^- and Δ^{++} resonances, as well as the resulting particle fractions and NS structure, may differ from conventional expectations. This suggests that a separate treatment of the kinetic and potential components of the symmetry energy could be relevant for describing certain NS properties [286].

Future studies could generalize such equations to include SRC-HMT effects on both the kinetic and potential symmetry energy, quantify how large kinetic terms influence the critical densities for Δ and hyperon formation, and assess the impact on NS composition and dynamical processes. In addition, it is important to explore how SRC-HMT affects in-medium Δ -nucleon and hyperon-nucleon interactions [287], to develop a self-consistent theoretical framework, and to investigate the connection with the in-medium pion and ρ meson properties [50, 51, 288], which could further influence the production and behavior of exotic particles in NS cores.

(5) Are There Clear Probes of SRC-HMT Effects in NSs?

The effects of SRC-HMT on NS properties are usually incorporated through modifications of the EOS in the literature. Specifically, studies often examine how observables such as the M-R relations, tidal deformabilities, and proton fractions respond to the inclusion of SRC-induced HMT effects (via the $n(k)$ in the quasi-particle picture). However, it is well known that the TOV equations are, in a sense, composition-blind: given any EOS, they can be integrated to produce M-R relations regardless of the underlying composition of the star. Consequently, the SRC-HMT effects could, in principle, be effectively mimicked by other physical ingredients in the EOS, raising a fundamental question: can we identify intrinsic and unambiguous probes that directly reveal the presence of SRC-HMT effects in NSs? We notice that similar questions can be raised about all possible new degrees of freedom or phases in NSs.

Identifying intrinsic and differentiable probes for SRC-HMT effects in NSs remains a crucial challenge. Recently, Ref. [289] showed that the magnetic-type Love number is a robust indicator for distinguishing NSs from quark stars (QSs), whereas the electric-type Love number may fail when QSs and NSs have similar masses and radii. In a similar spirit, it is necessary to go beyond simply exploring EOS modifications and seek observables that can uniquely and unambiguously reveal SRC-HMT effects, providing a pathway to directly detect and constrain these SRCs in NS interiors.

D Summary

In summary of this brief review, we emphasize the following among many interesting physics in this exciting field:

- **Microscopic origin of SRC-HMTs:** Nucleon SRCs, generated by the tensor and short-range components of the nuclear force, deplete the Fermi sea and produce a characteristic HMT in the single-nucleon momentum distribution, approximately following a universal k^{-4} behavior and dominated by neutron-proton isosinglet pairs.
- **Modification of the kinetic EOS:** SRC-HMTs substantially alter the kinetic contribution to the dense-matter EOS, stiffening the kinetic energy of symmetric nuclear matter while strongly reducing the kinetic symmetry energy and generating a sizable isospin-quartic term in the EOS of ANM.
- **Rearrangement of the potential contribution:** To satisfy empirical constraints near saturation density, the potential part of the EOS must compensate for SRC-induced kinetic effects, leading to significant changes in the density dependence of both isoscalar and isovector interaction channels.
- **Implications for NS properties:** At supranuclear densities relevant to NS interiors, SRC-HMT effects modify the proton fraction, the pressure-energy relation, and TOV solutions, thereby impacting the maximum NS mass, direct URCA cooling thresholds, crust-core transition density, transport properties, critical appearance densities of new particles and phases, and tidal responses in a currently model-dependent manner.
- **Open issues and future outlook:** The density and isospin dependence of SRCs above saturation density remain largely unconstrained, leaving open questions regarding their roles in NS cores and inner crusts, exotic degrees of

freedom, in-medium pion and ρ -meson dynamics, and higher-order EOS coefficients; addressing these challenges requires coordinated advances in *ab initio* nuclear many-body theory, heavy-ion reaction experiments, and multi-messenger astrophysics.

Acknowledgment

We would like to thank Rui Wang for helpful discussions. This work was supported in part by the National Natural Science Foundation of China under contract No. 12547102, the U.S. Department of Energy, Office of Science, under Award Number DE-SC0013702, the CUSTIPEN (China-U.S. Theory Institute for Physics with Exotic Nuclei) under the US Department of Energy Grant No. DE-SC0009971.

References

- [1] J.D Walecka. A theory of highly condensed matter. *Annals of Physics*, 83(2):491–529, 1974.
- [2] J. C. Collins and M. J. Perry. Superdense matter: Neutrons or asymptotically free quarks? *Phys. Rev. Lett.*, 34:1353–1356, May 1975.
- [3] S.A. Chin. A relativistic many-body theory of high density matter. *Annals of Physics*, 108(2):301–367, 1977.
- [4] Barry A. Freedman and Larry D. McLerran. Fermions and gauge vector mesons at finite temperature and density. i. formal techniques. *Phys. Rev. D*, 16:1130–1146, Aug 1977.
- [5] Barry A. Freedman and Larry D. McLerran. Fermions and gauge vector mesons at finite temperature and density. ii. the ground-state energy of a relativistic electron gas. *Phys. Rev. D*, 16:1147–1168, Aug 1977.
- [6] Barry A. Freedman and Larry D. McLerran. Fermions and gauge vector mesons at finite temperature and density. iii. the ground-state energy of a relativistic quark gas. *Phys. Rev. D*, 16:1169–1185, Aug 1977.
- [7] Varouzhan Baluni. Non-abelian gauge theories of fermi systems: Quantum-chromodynamic theory of highly condensed matter. *Phys. Rev. D*, 17:2092–2121, Apr 1978.
- [8] R. B. Wiringa, V. Fiks, and A. Fabrocini. Equation of state for dense nucleon matter. *Phys. Rev. C*, 38:1010–1037, Aug 1988.
- [9] A. Akmal, V. R. Pandharipande, and D. G. Ravenhall. Equation of state of nucleon matter and neutron star structure. *Phys. Rev. C*, 58:1804–1828, Sep 1998.
- [10] A. B. Migdal. Pion fields in nuclear matter. *Rev. Mod. Phys.*, 50:107–172, Jan 1978.
- [11] Edward V. Shuryak. Quantum chromodynamics and the theory of superdense matter. *Physics Reports*, 61(2):71–158, 1980.
- [12] D. Bailin and A. Love. Superfluidity and superconductivity in relativistic fermion systems. *Physics Reports*, 107(6):325–385, 1984.
- [13] J. M. Lattimer and M. Prakash. Neutron star structure and the equation of state. *The Astrophysical Journal*, 550(1):426, mar 2001.
- [14] Pawe Danielewicz, Roy Lacey, and William G. Lynch. Determination of the equation of state of dense matter. *Science*, 298(5598):15921596, November 2002.
- [15] A.W. Steiner, M. Prakash, J.M. Lattimer, and PJ. Ellis. Isospin asymmetry in nuclei and neutron stars. *Physics Reports*, 411(6):325–375, 2005.
- [16] Bao-An Li, Lie-Wen Chen, and Che Ming Ko. Recent progress and new challenges in isospin physics with heavy-ion reactions. *Physics Reports*, 464(4):113–281, 2008.
- [17] Mark G. Alford, Andreas Schmitt, Krishna Rajagopal, and Thomas Schäfer. Color superconductivity in dense quark matter. *Rev. Mod. Phys.*, 80:1455–1515, Nov 2008.
- [18] Anna L. Watts, Nils Andersson, Deepo Chakrabarty, Marco Feroci, Kai Hebeler, Gianluca Israel, Frederick K. Lamb, M. Coleman Miller, Sharon Morsink, Feryal Özel, Alessandro Patruno, Juri Poutanen, Dimitrios Psaltis, Achim Schwenk, Andrew W. Steiner, Luigi Stella, Laura Tolos, and Michiel van der Klis. Colloquium: Measuring the neutron star equation of state using x-ray timing. *Rev. Mod. Phys.*, 88:021001, Apr 2016.
- [19] Feryal Özel and Paulo Freire. Masses, Radii, and the Equation of State of Neutron Stars. *Ann. Rev. Astron. Astrophys.*, 54:401–440, September 2016.
- [20] M. Oertel, M. Hempel, T. Klähn, and S. Typel. Equations of state for supernovae and compact stars. *Rev. Mod. Phys.*, 89:015007, Mar 2017.
- [21] Isaac Vidaña. Hyperons: the strange ingredients of the nuclear equation of state. *Proceedings of the Royal Society of London Series A*, 474(2217):20180145, September 2018.
- [22] G.F. Burgio, H.-J. Schulze, I. Vidaña, and J.-B. Wei. Neutron stars and the nuclear equation of state. *Progress in Particle and Nuclear Physics*, 120:103879, 2021.
- [23] C. Drischler, J.W. Holt, and C. Wellenhofer. Chiral effective field theory and the high-density nuclear equation of state. *Annual Review of Nuclear and Particle Science*, 71(1):403432, September 2021.
- [24] Sorensen Agnieszka et al. Dense nuclear matter equation of state from heavy-ion collisions. *Progress in Particle and Nuclear Physics*, 134:104080, 2024.
- [25] Rajesh Kumar et al. Theoretical and experimental constraints for the equation of state of dense and hot matter. *Living Reviews in Relativity*, 27(1), June 2024.
- [26] Gordon Baym, Tetsuo Hatsuda, Toru Kojo, Philip D Powell, Yifan Song, and Tatsuyuki Takatsuka. From hadrons to quarks in neutron stars: a review. *Reports on Progress in Physics*, 81(5):056902, mar 2018.
- [27] Luca Baiotti. Gravitational waves from neutron star mergers and their relation to the nuclear equation of state. *Progress in Particle and Nuclear Physics*, 109:103714, 2019.
- [28] Milva G Orsaria, Germán Malfatti, Mauro Mariani, Ignacio F Ranea-Sandoval, Federico García, William M Spinella, Gustavo A Contrera, Germán Lugones, and Fridolin Weber. Phase transitions in neutron stars and their links to gravitational waves. *Journal of Physics G: Nuclear and Particle Physics*, 46(7):073002, jun 2019.
- [29] Bao-An Li, Plamen G. Krastev, De-Hua Wen, and Nai-Bo Zhang. Towards understanding astrophysical effects of nuclear symmetry energy. *The European Physical Journal A*, 55(7), July 2019.
- [30] V Dexheimer, J Noronha, J Noronha-Hostler, N Yunes, and C Ratti. Future physics perspectives on the equation of state from heavy ion collisions to neutron stars. *Journal of Physics G: Nuclear and Particle Physics*, 48(7):073001, may 2021.
- [31] J. M. Lattimer. Neutron Stars and the Nuclear Matter Equation of State. *Ann. Rev. Nucl. Part. Sci.*, 71:433–464, 2021.

[32] Jin-Hui Chen et al. Properties of the qcd matter: review of selected results from the relativistic heavy ion collider beam energy scan (rhic bes) program. *Nuclear Science and Techniques*, 35(12), November 2024.

[33] Qi-Ye Shou, Yu-Gang Ma, Song Zhang, Jian-Hui Zhu, Ya-Xian Mao, Hua Pei, Zhong-Bao Yin, Xiao-Ming Zhang, Dai-Cui Zhou, Xin-Ye Peng, Xiao-Zhi Bai, Ze-Bo Tang, Yi-Fei Zhang, and Xiao-Mei Li. Properties of qcd matter: a review of selected results from alice experiment. *Nuclear Science and Techniques*, 35(12), December 2024.

[34] Meng-Qi Ding, De-Qing Fang, and Yu-Gang Ma. Neutron skin and its effects in heavy-ion collisions. *Nuclear Science and Techniques*, 35(12):211, December 2024.

[35] S. Shapiro and S. Teukolsky. *Black Holes, White Dwarfs and Neutron Stars: the Physics of Compact Objects*. Wiley-VCH, 1983.

[36] P. Haensel, A. Y. Potekhin, and D. G. Yakovlev. *Neutron stars 1: Equation of state and structure*, volume 326. Springer, New York, USA, 2007.

[37] Bao-Jun Cai and Bao-An Li. Novel scalings of neutron star properties from analyzing dimensionless tolmanoppenheimervolkoff equations. *The European Physical Journal A*, 61(3), March 2025.

[38] N. Brambilla et al. QCD and Strongly Coupled Gauge Theories: Challenges and Perspectives. *Eur. Phys. J. C*, 74(10):2981, 2014.

[39] Stefano Giorgini, Lev P. Pitaevskii, and Sandro Stringari. Theory of ultracold atomic fermi gases. *Rev. Mod. Phys.*, 80:1215–1274, Oct 2008.

[40] Immanuel Bloch, Jean Dalibard, and Wilhelm Zwerger. Many-body physics with ultracold gases. *Rev. Mod. Phys.*, 80:885–964, Jul 2008.

[41] O. Hen, G. A. Miller, E. Piasetzky, and L. B. Weinstein. Nucleon-Nucleon Correlations, Short-lived Excitations, and the Quarks Within. *Rev. Mod. Phys.*, 89(4):045002, 2017.

[42] H. A. Bethe. Theory of nuclear matter. *Ann. Rev. Nucl. Part. Sci.*, 21:93–244, 1971.

[43] Shina Tan. Energetics of a strongly correlated fermi gas. *Annals of Physics*, 323(12):29522970, December 2008.

[44] Shina Tan. Large momentum part of a strongly correlated fermi gas. *Annals of Physics*, 323(12):29712986, December 2008.

[45] Shina Tan. Generalized virial theorem and pressure relation for a strongly correlated Fermi gas. *Annals Phys.*, 323:2987–2990, 2008.

[46] O. Hen et al. Momentum sharing in imbalanced Fermi systems. *Science*, 346(6209):614–617, October 2014.

[47] R. Subedi et al. Probing cold dense nuclear matter. *Science*, 320(5882):14761478, June 2008.

[48] O. Benhar, V. R. Pandharipande, and Steven C. Pieper. Electron-scattering studies of correlations in nuclei. *Rev. Mod. Phys.*, 65:817–828, Jul 1993.

[49] E. I. Piasetzky and L. B. Weinstein. *Measurements of NN Correlations in Nuclei*, pages 2385–2406. Springer Nature Singapore, Singapore, 2023.

[50] Torleif Erik Oskar Ericson and W. Weise. *Pions and Nuclei*. Clarendon Press, Oxford, UK, 1988.

[51] G. E. Brown and Mannque Rho. In-medium stiffening of the nucleon nucleon spin - isospin interaction. *Phys. Lett. B*, 237:3–7, 1990.

[52] Sigfrido Boffi, Carlotta Giusti, Franco davide Pacati, and Marco Radici. *Electromagnetic Response of Atomic Nuclei*, volume 20 of *Oxford Studies in Nuclear Physics*. Clarendon Press, Oxford UK, 1996.

[53] J. J. Aubert et al. The ratio of the nucleon structure functions F_{2n} for iron and deuterium. *Phys. Lett. B*, 123:275–278, 1983.

[54] L. B. Weinstein, E. Piasetzky, D. W. Higinbotham, J. Gomez, O. Hen, and R. Shneor. Short Range Correlations and the EMC Effect. *Phys. Rev. Lett.*, 106:052301, 2011.

[55] B. Schmookler et al. Modified structure of protons and neutrons in correlated pairs. *Nature*, 566(7744):354–358, 2019.

[56] Bao-An Li, Wen-Jun Guo, and Zhaozhong Shi. Effects of the kinetic symmetry energy reduced by short-range correlations in heavy-ion collisions at intermediate energies. *Phys. Rev. C*, 91:044601, Apr 2015.

[57] I. Bombaci and U. Lombardo. Asymmetric nuclear matter equation of state. *Phys. Rev. C*, 44:1892–1900, Nov 1991.

[58] Bao-Jun Cai and Lie-Wen Chen. Nuclear matter fourth-order symmetry energy in the relativistic mean field models. *Phys. Rev. C*, 85:024302, Feb 2012.

[59] W. M. Seif and D. N. Basu. Higher-order symmetry energy of nuclear matter and the inner edge of neutron star crusts. *Phys. Rev. C*, 89:028801, Feb 2014.

[60] C. Gonzalez-Boquera, M. Centelles, X. Viñas, and A. Rios. Higher-order symmetry energy and neutron star core-crust transition with gogny forces. *Phys. Rev. C*, 96:065806, Dec 2017.

[61] Jie Pu, Zhen Zhang, and Lie-Wen Chen. Nuclear matter fourth-order symmetry energy in nonrelativistic mean-field models. *Phys. Rev. C*, 96:054311, Nov 2017.

[62] Bao-An Li, Bao-Jun Cai, Lie-Wen Chen, and Jun Xu. Nucleon effective masses in neutron-rich matter. *Progress in Particle and Nuclear Physics*, 99:29119, March 2018.

[63] D. Ding, A. Rios, H. Dussan, W. H. Dickhoff, S. J. Witte, A. Carbone, and A. Polls. Pairing in high-density neutron matter including short- and long-range correlations. *Phys. Rev. C*, 94:025802, Aug 2016.

[64] B. P. Abbott et al. Gw170817: Observation of gravitational waves from a binary neutron star inspiral. *Phys. Rev. Lett.*, 119:161101, Oct 2017.

[65] B. P. Abbott et al. Gw170817: Measurements of neutron star radii and equation of state. *Phys. Rev. Lett.*, 121:161101, Oct 2018.

[66] B.P. Abbott et al. Gw190425: Observation of a compact binary coalescence with total mass $3.4m_{\odot}$. *The Astrophysical Journal Letters*, 892(1):L3, mar 2020.

[67] R. Abbott et al. Gw190814: Gravitational waves from the coalescence of a 23 solar mass black hole with a 2.6 solar mass compact object. *The Astrophysical Journal Letters*, 896(2):L44, jun 2020.

[68] E. Riley Thomas et al. A nicer view of the massive pulsar psr j0740+6620 informed by radio timing and xmm-newton spectroscopy. *The Astrophysical Journal Letters*, 918(2):L27, sep 2021.

[69] T. E. Riley et al. A nicer view of psr j0030+0451: Millisecond pulsar parameter estimation. *The Astrophysical Journal Letters*, 887(1):L21, dec 2019.

[70] Devarshi Choudhury et al. A nicer view of the nearest and brightest millisecond pulsar: Psr j04374715. *The Astrophysical Journal Letters*, 971(1):L20, August 2024.

[71] Lucien Mauviard, Sebastien Guillot, Tuomo Salmi, Devarshi Choudhury, Bas Dorsman, Denis González-Caniulef, Mariska Hoogkamer, Daniela Huppenkothen, Christine Kazantsev, Yves Kini, Jean-Francois Olive, Pierre Stammle, Anna L. Watts, Melissa Mendes, Nathan Rutherford, Achim Schwenk, Isak Svensson, Slavko Bogdanov, Matthew Kerr, Paul S. Ray, Lucas Guillemot, Ismaël Cognard, and Gilles Theureau. A nicer view of the 1.4 solar-mass edge-on pulsar psr j0614–3329, 2025. arXiv:2506.14883.

[72] Andrew G. Sullivan and Roger W. Romani. The intrabinary shock and companion star of redback pulsar j2215+5135. *The Astrophysical Journal*, 974(2):315, October 2024.

[73] Roger W. Romani, D. Kandel, Alexei V. Filippenko, Thomas G. Brink, and WeiKang Zheng. Psr j09520607: The fastest and heaviest known galactic neutron star. *The Astrophysical Journal Letters*, 934(2):L17, July 2022.

[74] P. B. Demorest, T. Pennucci, S. M. Ransom, M. S. E. Roberts, and J. W. T. Hessels. A two-solar-mass neutron star measured using shapiro delay. *Nature*, 467(7319):10811083, October 2010.

[75] Zaven Arzoumanian et al. The nanograv 11-year data set: High-precision timing of 45 millisecond pulsars. *The Astrophysical Journal Supplement Series*, 235(2):37, April 2018.

[76] John Antoniadis et al. A massive pulsar in a compact relativistic binary. *Science*, 340(6131), April 2013.

[77] E. Fonseca et al. Refined mass and geometric measurements of the high-mass psr j0740+6620. *The Astrophysical Journal Letters*, 915(1):L12, jul 2021.

[78] M. C. Miller et al. The radius of psr j0740+6620 from nicer and xmm-newton data. *The Astrophysical Journal Letters*, 918(2):L28, sep 2021.

[79] Tuomo Salmi et al. The radius of psr j0740+6620 from nicer with nicer background estimates. *The Astrophysical Journal*, 941(2):150, dec 2022.

[80] Tuomo Salmi et al. The radius of the high mass pulsar psr j0740+6620 with 3.6 years of nicer data. *Astrophysical J.*, 2024.

[81] Alexander J. Dittmann et al. =. A more precise measurement of the radius of psr j0740+6620 using updated nicer data. *Astrophysical Journal*, 2024.

[82] M. C. Miller et al. Psr j0030+0451 mass and radius from nicer data and implications for the properties of neutron star matter. *The Astrophysical Journal Letters*, 887(1):L24, dec 2019.

[83] Serena Vinciguerra et al. An updated massradius analysis of the 20172018 nicer data set of psr j0030+0451. *The Astrophysical Journal*, 961(1):62, jan 2024.

[84] Daniel J. Reardon et al. The neutron star mass, distance, and inclination from precision timing of the brilliant millisecond pulsar j0437-4715. *The Astrophysical Journal Letters*, 971(1):L18, August 2024.

[85] D Yakovlev. Neutrino emission from neutron stars. *Physics Reports*, 354(12):1155, November 2001.

[86] J. M. Dong, U. Lombardo, H. F. Zhang, and W. Zuo. Role of nucleonic fermi surface depletion in neutron star cooling. *The Astrophysical Journal*, 817(1):6, January 2016.

[87] Armen Sedrakian. Short-range correlations and urca process in neutron stars. *Phys. Rev. Lett.*, 133:171401, Oct 2024.

[88] W.H. Dickhoff and C. Barbieri. Self-consistent greens function method for nuclei and nuclear matter. *Progress in Particle and Nuclear Physics*, 52(2):377496, April 2004.

[89] Nadia Fomin, Douglas Higinbotham, Misak Sargsian, and Patricia Solvignon. New Results on Short-Range Correlations in Nuclei. *Annual Review of Nuclear and Particle Science*, 67:129–159, October 2017.

[90] J. Arrington, D.W. Higinbotham, G. Rosner, and M. Sargsian. Hard probes of short-range nucleonnucleon correlations. *Progress in Particle and Nuclear Physics*, 67(4):898938, October 2012.

[91] J. Arrington, M. Battaglieri, A. Boehnlein, S. A. Bogacz, W. K. Brooks, E. Chudakov, I. Cloet, R. Ent, H. Gao, J. Grames, L. Harwood, X. Ji, C. Keppel, G. Krafft, R. D. McKeown, J. Napolitano, J. W. Qiu, P. Rossi, M. Schram, S. Stepanyan, J. Stevens, A. P. Szczepaniak, N. Toro, and X. Zheng. Physics with cebaf at 12 gev and future opportunities, 2022. arXiv:2112.00060.

[92] John Arrington, Nadia Fomin, and Axel Schmidt. Progress in understanding short-range structure in nuclei: An experimental perspective. *Annual Review of Nuclear and Particle Science*, 72(1):307337, September 2022.

[93] Ranjeet Dalal and I. J. Douglas MacGregor. Nucleon-nucleon correlations inside atomic nuclei: synergies, observations and theoretical models, 2022. arXiv:2210.06114.

[94] T. Aumann, C. Barbieri, D. Bazin, C.A. Bertulani, A. Bonaccorso, W.H. Dickhoff, A. Gade, M. Gómez-Ramos, B.P. Kay, A.M. Moro, T. Nakamura, A. Obertelli, K. Ogata, S. Paschalidis, and T. Uesaka. Quenching of single-particle strength from direct reactions with stable and rare-isotope beams. *Progress in Particle and Nuclear Physics*, 118:103847, May 2021.

[95] L.L. Frankfurt and M.I. Strikman. Qcd and short-range nuclear phenomena. *Nuclear Physics B*, 181(1):22–60, 1981.

[96] L. L. Frankfurt and M. I. Strikman. Hard Nuclear Processes and Microscopic Nuclear Structure. *Phys. Rept.*, 160:235–427, 1988.

[97] Claudio Ciofi degli Atti. In-medium short-range dynamics of nucleons: Recent theoretical and experimental advances. *Physics Reports*, 590:1–85, 2015. In-medium short-range dynamics of nucleons: Recent theoretical and experimental advances.

[98] LEONID FRANKFURT, MISAK SARGSIAN, and MARK STRIKMAN. Recent observation of short-range nucleon correlations in nuclei and their implications for the structure of nuclei and neutron stars. *International Journal of Modern Physics A*, 23(20):29913055, August 2008.

[99] Bao-Jun Cai, Bao-An Li, and Yu-Gang Ma. Nucleon short-range correlations and high-momentum dynamics: Implications on the equation of state of dense matter, 2025. arXiv:2512.04206.

[100] Bao-Jun Cai and Bao-An Li. Symmetry energy of cold nucleonic matter within a relativistic mean field model encapsulating effects of high-momentum nucleons induced by short-range correlations. *Phys. Rev. C*, 93:014619, Jan 2016.

[101] Bao-Jun Cai and Bao-An Li. Isospin quartic term in the kinetic energy of neutron-rich nucleonic matter. *Physical Review C*, 92(1), July 2015.

[102] Bao-Jun Cai and Bao-An Li. Nucleon effective E-mass in neutron-rich matter from the Migdal-Luttinger jump. *Phys. Lett. B*, 757:79–83, 2016.

[103] Bao-Jun Cai, Bao-An Li, and Lie-Wen Chen. Proton skins in momentum space and neutron skins in coordinate space in heavy nuclei. *Phys. Rev. C*, 94:061302, Dec 2016.

[104] A.B. Migdal. The momentum distribution of interacting fermi particles. *JETP*, 5:333, 1957.

[105] J. M. Luttinger. Fermi Surface and Some Simple Equilibrium Properties of a System of Interacting Fermions. *Physical Review*, 119(4):1153–1163, August 1960.

[106] C. Mahaux, P. F. Bortignon, R. A. Broglia, and C. H. Dasso. Dynamics of the shell model. *Phys. Rept.*, 120:1–274, 1985.

[107] M. Jaminon and C. Mahaux. Effective masses in relativistic approaches to the nucleon-nucleus mean field. *Phys. Rev. C*, 40:354–367, Jul 1989.

[108] V.A. Belyakov. The momentum distribution of interacting fermi particles. *JETP*, 13:850, 1961.

[109] W. Czy and K. Gottfried. The momentum distribution in a dilute fermi gas at zero temperature. *Nuclear Physics*, 21:676–680, 1960.

[110] R. Sartor and C. Mahaux. Self-energy, momentum distribution, and effective masses of a dilute Fermi gas. *Phys. Rev. C*, 21:1546–1567, 1980. [Erratum: Phys.Rev.C 25, 677–677 (1982)].

[111] A.N. Antonov, P.E. Hodgson, and I.Z. Petkov. *Nucleon Momentum and Density Distributions in Nuclei*. Oxford science publications. Clarendon Press, 1988.

[112] Ronen Weiss, Betzalel Bazak, and Nir Barnea. Generalized nuclear contacts and momentum distributions. *Phys. Rev. C*, 92:054311, Nov 2015.

[113] O. Hen, L. B. Weinstein, E. Piasetzky, G. A. Miller, M. M. Sargsian, and Y. Sagi. Correlated fermions in nuclei and ultracold atomic gases. *Phys. Rev. C*, 92:045205, Oct 2015.

[114] Or Hen, Bao-An Li, Wen-Jun Guo, L. B. Weinstein, and Eli Piasetzky. Symmetry energy of nucleonic matter with tensor correlations. *Phys. Rev. C*, 91:025803, Feb 2015.

[115] Bernard Frois and Costas N. Papanicolas. Electron Scattering and Nuclear Structure. *Ann. Rev. Nucl. Part. Sci.*, 37:133–176, 1987.

[116] Florian Hauenstein, Julian Kahlbow, and Or Hen. From quarks to nuclei: Short range correlations studies across the globe. *Nuclear Physics News*, 31(1):19–24, 2021.

[117] O. Hen, D. W. Higinbotham, E. Piazetsky, and A. Schmidt. Topical issue on short-range correlations and the EMC effect. *Eur. Phys. J. A*, 61(5):109, 2025.

[118] Zhoudunming Tu, Alexander Jentsch, Mark Baker, Liang Zheng, Jeong-Hun Lee, Raju Venugopalan, Or Hen, Douglas Higinbotham, Elke-Caroline Aschenauer, and Thomas Ullrich. Probing short-range correlations in the deuteron via incoherent diffractive J/ψ production with spectator tagging at the EIC. *Phys. Lett. B*, 811:135877, 2020.

[119] F. Hauenstein et al. Measuring recoiling nucleons from the nucleus with the future Electron Ion Collider. *Phys. Rev. C*, 105(3):034001, 2022.

[120] Daniel Boer et al. Gluons and the quark sea at high energies: Distributions, polarization, tomography. *ArXiv: 1108.1713*, August 2011.

[121] R3b src proposal. https://indico.ph.tum.de/event/7050/contributions/6385/attachments/4485/5708/NuPECC_SRC.pdf, 2025.

[122] Hang Qi, Julian Kahlbow, and R3B S522 Collaboration Team. Short-Range Correlation Studies in Inverse Kinematics to access unstable nuclei. In *APS Meeting Abstracts*, APS Meeting Abstracts, page E11.003, January 2023.

[123] Fair website. <https://fair-center.eu/>, 2025.

[124] Zhihong Ye, Haojie Zhang, Yaopeng Zhang, and Haocen Zhao. New Chinese facilities for short-range correlation physics. *Eur. Phys. J. A*, 60(6):126, 2024.

[125] Daniele P. Anderle et al. Electron-ion collider in china. *Frontiers of Physics*, 16(6), June 2021.

[126] Julian Kahlbow. Study of SRCs in neutron-rich nuclei with inverse kinematics measurements. *Eur. Phys. J. A*, 59(6):128, 2023.

[127] John Arrington, Reynier Cruz-Torres, Tyler J. Hague, Leiqaa Kurbany, Shujie Li, David Meekins, and Nathaly Santiesteban. The Jefferson Lab tritium program of nucleon and nuclear structure measurements. *European Physical Journal A*, 59(8):188, August 2023.

[128] Nadia Fomin, John Arrington, and Shujie Li. Searching for three-nucleon short-range correlations. *European Physical Journal A*, 59(9):205, September 2023.

[129] Xu Junhuai et al. Precise measurement of short-range correlations in nuclei from bremsstrahlung gamma-ray emission in low-energy heavy-ion collisions. *Phys. Rev. Res.*, 7:043174, Nov 2025.

[130] N. Fomin et al. New measurements of high-momentum nucleons and short-range structures in nuclei. *Phys. Rev. Lett.*, 108:092502, Feb 2012.

[131] L. B. Weinstein, E. Piasetzky, D. W. Higinbotham, J. Gomez, O. Hen, and R. Shneor. Short range correlations and the emc effect. *Phys. Rev. Lett.*, 106:052301, Feb 2011.

[132] K. S. Egiyan et al. Measurement of two- and three-nucleon short-range correlation probabilities in nuclei. *Phys. Rev. Lett.*, 96:082501, Mar 2006.

[133] L. L. Frankfurt, M. I. Strikman, D. B. Day, and M. Sargsyan. Evidence for short-range correlations from high q^2 (e, e') reactions. *Phys. Rev. C*, 48:2451–2461, Nov 1993.

[134] Misak M. Sargsian. New properties of the high-momentum distribution of nucleons in asymmetric nuclei. *Phys. Rev. C*, 89:034305, Mar 2014.

[135] S. Fantoni and V. R. Pandharipande. Momentum distribution of nucleons in nuclear matter. *Nucl. Phys. A*, 427:473–492, 1984.

[136] Steven C. Pieper, R. B. Wiringa, and V. R. Pandharipande. Variational calculation of the ground state of ^{16}O . *Phys. Rev. C*, 46:1741–1756, Nov 1992.

[137] C. Ciofi degli Atti and S. Simula. Realistic model of the nucleon spectral function in few- and many-nucleon systems. *Phys. Rev. C*, 53:1689–1710, Apr 1996.

[138] Rong Wang, Xu-Rong Chen, and Tao-Feng Wang. Mass of a short-range correlated nucleon *. *Chinese Physics C*, 45(2):021001, February 2021.

[139] Michael McGauley and Misak M. Sargsian. Off-fermi shell nucleons in superdense asymmetric nuclear matter, 2012. *arXiv:1102.3973*.

[140] C. Ciofi degli Atti, E. Pace, and G. Salmè. y -scaling analysis of quasielastic electron scattering and nucleon momentum distributions in few-body systems, complex nuclei, and nuclear matter. *Phys. Rev. C*, 43:1155–1176, Mar 1991.

[141] Hongkai Dai, Rong Wang, Yin Huang, and Xurong Chen. A novel nuclear dependence of nucleon-nucleon short-range correlations. *Physics Letters B*, 769:446–450, 2017.

[142] Ronen Weiss, Betzalel Bazak, and Nir Barnea. Generalized nuclear contacts and momentum distributions. *Phys. Rev. C*, 92:054311, Nov 2015.

[143] R. Cruz-Torres et al. Many-body factorization and position-momentum equivalence of nuclear short-range correlations. *Nature Phys.*, 17(3):306–310, 2021.

[144] W. Cosyn and J. Ryckebusch. Phase-space distributions of nuclear short-range correlations. *Physics Letters B*, 820:136526, September 2021.

[145] Tongqi Liang, Dong Bai, and Zhongzhou Ren. Nuclear contacts of unstable nuclei. *Physics Letters B*, 857:138965, October 2024.

[146] Tongqi Liang, Dong Bai, and Zhongzhou Ren. Universal laws for nuclear contacts. 2024.

[147] X. G. Wang, A. W. Thomas, and W. Melnitchouk. Do short-range correlations cause the nuclear emc effect in the deuteron? *Phys. Rev. Lett.*, 125:262002, Dec 2020.

[148] Ani Aprahamian et al. Reaching for the horizon: The 2015 long range plan for nuclear science. 10 2015.

[149] A. Rios, A. Polls, and W. H. Dickhoff. Density and isospin-asymmetry dependence of high-momentum components. *Phys. Rev. C*, 89:044303, Apr 2014.

[150] Maarten Vanhalst, Jan Ryckebusch, and Wim Cosyn. Quantifying short-range correlations in nuclei. *Physical Review C*, 86(4), October 2012.

[151] Maarten Vanhalst, Wim Cosyn, and Jan Ryckebusch. Counting the number of correlated pairs in a nucleus. *Physical Review C*, 84(3), September 2011.

[152] Jan Ryckebusch, Wim Cosyn, Tom Viejra, and Corneel Casert. Isospin composition of the high-momentum fluctuations in nuclei from asymptotic momentum distributions. *Phys. Rev. C*, 100:054620, Nov 2019.

[153] J E Lynn, D Lonardoni, J Carlson, J-W Chen, W Detmold, S Gandolfi, and A Schwenk. Ab initio short-range-correlation scaling factors from light to medium-mass nuclei. *Journal of Physics G: Nuclear and Particle Physics*, 47(4):045109, March 2020.

[154] W.H. VAN NECK DICKHOFF and D.V.Y. Van Neck. *Many-Body Theory Exposed!: Propagator Description of Quantum Mechanics in Many-Body Systems (Third Edition)*. World Scientific Publishing Company, 2025.

[155] E. Piasetzky, M. Sargsian, L. Frankfurt, M. Strikman, and J. W. Watson. Evidence for strong dominance of proton-neutron correlations in nuclei. *Phys. Rev. Lett.*, 97:162504, Oct 2006.

[156] R. Shneor et al. Investigation of proton-proton short-range correlations via the $^{12}\text{C}(e, e' pp)$ reaction. *Phys. Rev. Lett.*, 99:072501, Aug 2007.

[157] I. Korover et al. Probing the repulsive core of the nucleon-nucleon interaction via the $^4\text{He}(e, e' pn)$ triple-coincidence reaction. *Phys. Rev. Lett.*, 113:022501, Jul 2014.

[158] Qinglin Niu, Jian Liu, Yuanlong Guo, Chang Xu, Mengjiao Lyu, and Zhongzhou Ren. Effects of nucleon-nucleon short-range correlations on inclusive electron scattering. *Phys. Rev. C*, 105:L051602, May 2022.

[159] R. Cruz-Torres, A. Schmidt, G.A. Miller, L.B. Weinstein, N. Barnea, R. Weiss, E. Piasetzky, and O. Hen. Short range correlations and the isospin dependence of nuclear correlation functions. *Physics Letters B*, 785:304–308, 2018.

[160] S. Paschalis, M. Petri, A. O. Macchiavelli, O. Hen, and E. Piasetzky. Nucleon-nucleon correlations and the single-particle strength in atomic nuclei. *Phys. Lett. B*, 800:135110, 2020.

[161] M. Duer et al. Probing high-momentum protons and neutrons in neutron-rich nuclei. *Nature*, 560(7720):617–621, 2018.

[162] S. Li et al. Revealing the short-range structure of the mirror nuclei 3h and 3he . *Nature*, 609(7925):4145, August 2022.

[163] R. Weiss, A. W. Denniston, J. R. Pybus, O. Hen, E. Piasetzky, A. Schmidt, L. B. Weinstein, and N. Barnea. Extracting the number of short-range correlated nucleon pairs from inclusive electron scattering data. *Phys. Rev. C*, 103:L031301, Mar 2021.

[164] Haoyu Shang, Jiawei Chen, Rongzhe Hu, Xin Zhen, Chongji Jiang, and Junchen Pei. Many-body effects on nuclear short range correlations. 2025. arXiv:2503.17119.

[165] Qi Meng, Ziyang Lu, and Chang Xu. Short-range correlations and momentum distributions in mirror nuclei ^3H and ^3He . *Phys. Rev. C*, 108:014001, Jul 2023.

[166] Bao-An Li, Bao-Jun Cai, Wen-Jie Xie, and Nai-Bo Zhang. Progress in constraining nuclear symmetry energy using neutron star observables since gw170817. *Universe*, 7(6), 2021.

[167] Bao-Jun Cai and Bao-An Li. Investigating effects of relativistic kinematics, dimensionality, interactions, and short-range correlations on the ratio of quartic over quadratic nuclear symmetry energies. *Phys. Rev. C*, 105:064607, Jun 2022.

[168] A. Carbone, A. Polls, and A. Rios. High-momentum components in the nuclear symmetry energy. *Europhysics Letters*, 97(2):22001, jan 2012.

[169] Isaac Vidaña, Artur Polls, and Constança Providência. Nuclear symmetry energy and the role of the tensor force. *Phys. Rev. C*, 84:062801, Dec 2011.

[170] Alessandro Lovato, Omar Benhar, Stefano Fantoni, Alexey Yu. Illarionov, and Kevin E. Schmidt. Density-dependent nucleon-nucleon interaction from three-nucleon forces. *Phys. Rev. C*, 83:054003, May 2011.

[171] Fang Zhang and Gao-Chan Yong. Effects of the high-momentum tail of nucleon momentum distribution on the isospin-sensitive observables. *European Physical Journal A*, 52(11):350, November 2016.

[172] Gao-Chan Yong. Constraining nucleon high momentum in nuclei. *Physics Letters B*, 765:104–108, 2017.

[173] Gao-Chan Yong and Bao-An Li. Interplay of short-range correlations and nuclear symmetry energy in hard-photon production from heavy-ion reactions at fermi energies. *Phys. Rev. C*, 96:064614, Dec 2017.

[174] Gao-Chan Yong. Probing proton transition momentum in neutron-rich matter. *Physics Letters B*, 776:447–450, 2018.

[175] Fang Zhang, Hai-Bo Peng, and Jiang-Tao Zhao. Isospin-sensitive observables as a probe of proton transition momentum in the hmt *. *Chinese Physics C*, 43(11):114106, nov 2019.

[176] Lei Shen, Bo-Song Huang, and Yu-Gang Ma. Short-range correlations in the extended quantum molecular dynamics model. *Phys. Rev. C*, 105:014603, Jan 2022.

[177] Wen-Mei Guo, Cui-Hua Chen, and Yu Lin. Probing heavy-ion collisions with the yield ratios of neutron-proton at intermediate energy. *Nucl. Phys. A*, 1033:122638, 2023.

[178] Wen-Mei Guo and Deng-Jie Li. Probing the surface properties of proton-rich nuclei with the yield ratios of neutrons and protons in intermediate-energy heavy-ion collisions. *Phys. Rev. C*, 110:064617, Dec 2024.

[179] Wen-Mei Guo, Bao-An Li, and Gao-Chan Yong. Interplay of effects of neutron skins in coordinate space and proton skins in momentum space on emission of hard photons in heavy-ion collisions near the fermi energy. *Phys. Rev. C*, 108:034617, Sep 2023.

[180] Wen-Mei Guo and Cui-Hua Chen. Effects of a high-momentum tail of the nucleon momentum distribution and in-medium nucleon-nucleon cross sections on nuclear stopping and collective flow in intermediate-energy heavy-ion collisions. *Phys. Rev. C*, 111:024612, Feb 2025.

[181] R. Wada, Q. Hu, G. Y. Tian, X. Q. Liu, W. P. Lin, J. H. Tan, and H. Zheng. High-energy neutron emission and short-range nucleon-nucleon correlations. *Phys. Rev. C*, 112:034614, Sep 2025.

[182] Tom Reichert and Jörg Aichelin. The influence of nuclear short range correlations on sub-threshold particle production in proton-nucleus collisions, 2025. arXiv:2506.03962.

[183] Junhuai Xu, Yuhao Qin, Zhi Qin, Dawei Si, Boyuan Zhang, Yijie Wang, Qinglin Niu, Chang Xu, and Zhigang Xiao. Reconstruction of bremsstrahlung -rays spectrum in heavy ion reactions with richardson-lucy algorithm. *Physics Letters B*, 857:139009, 2024.

[184] Bao-Jun Cai and Bao-An Li. Nuclear equation of state and single-nucleon potential from gogny-like energy density functionals encapsulating effects of nucleon-nucleon short-range correlations, 2022. arXiv:2210.10924.

[185] Lie-Wen Chen, Che Ming Ko, and Bao-An Li. Determination of the stiffness of the nuclear symmetry energy from isospin diffusion. *Phys. Rev. Lett.*, 94:032701, Jan 2005.

[186] Jun Xu and Che Ming Ko. Density matrix expansion for the isospin- and momentum-dependent mdi interaction. *Phys. Rev. C*, 82:044311, Oct 2010.

[187] Jun Xu, Lie-Wen Chen, and Bao-An Li. Thermal properties of asymmetric nuclear matter with an improved isospin- and momentum-dependent interaction. *Phys. Rev. C*, 91:014611, Jan 2015.

[188] B. Serot and J. Walecka. *The Relativistic Nuclear Many Body Problem*. *Advances in Nuclear Physics*, 16:1–327, 1986.

[189] Horst Müller and Brian D. Serot. Relativistic mean-field theory and the high-density nuclear equation of state. *Nuclear Physics A*, 606(34):508537, September 1996.

[190] Ying Cui, Yuan Tian, Cheng-Jun Xia, Ying-Xun Zhang, and Zhu-Xia Li. Constraint on the symmetry energy at high densities from neutron star observations using relativistic mean-field models. *Nuclear Science and Techniques*, 36(8):141, August 2025.

[191] M. B. Tsang et al. Constraints on the symmetry energy and neutron skins from experiments and theory. *Phys. Rev. C*, 86:015803, Jul 2012.

[192] Paweł Danielewicz and Jenny Lee. Symmetry energy ii: Isobaric analog states. *Nuclear Physics A*, 922:170, February 2014.

[193] Fan Li, Bao-Jun Cai, Ying Zhou, Wei-Zhou Jiang, and Lie-Wen Chen. Effects of isoscalar- and isovector-scalar meson mixing on neutron star structure. *The Astrophysical Journal*, 929(2):183, April 2022.

[194] Zhigang Xiao, Bao-An Li, Lie-Wen Chen, Gao-Chan Yong, and Ming Zhang. Circumstantial evidence for a soft nuclear symmetry energy at suprasaturation densities. *Phys. Rev. Lett.*, 102:062502, Feb 2009.

[195] Jun-Ting Ye, Rui Wang, Si-Pei Wang, and Lie-Wen Chen. High density symmetry energy: A key to the solution of the hyperon puzzle, 2025. arXiv:2411.18349.

[196] Si-Pei Wang, Xin Li, Rui Wang, Jun-Ting Ye, and Lie-Wen Chen. Extended skyrme effective interactions with higher-order momentum-dependence for transport models and neutron stars, 2025. arXiv:2412.09393.

[197] Si-Pei Wang and Lie-Wen Chen. Extended momentum-dependent interaction for transport models and neutron stars, 2025. arXiv:2507.02448.

[198] D. Adhikari et al. Accurate determination of the neutron skin thickness of ^{208}Pb through parity-violation in electron scattering. *Phys. Rev. Lett.*, 126:172502, Apr 2021.

[199] Nai-Bo Zhang and Bao-An Li. Impact of symmetry energy on sound speed and spinodal decomposition in dense neutron-rich matter. *Eur. Phys. J. A*, 59(4):86, 2023.

[200] Jun-Ting Ye, Rui Wang, Si-Pei Wang, and Lie-Wen Chen. High-density Symmetry Energy: A Key to the Solution of the Hyperon Puzzle. *Astrophys. J.*, 985(2):238, 2025.

[201] Bao-Jun Cai and Bao-An Li. Equation of state of neutron-rich matter in d-dimensions. *Annals of Physics*, 444:169062, 2022.

[202] Lev Pitaevskii and Sandro Stringari. *Bose-Einstein Condensation and Superfluidity*. Oxford University Press, 01 2016.

[203] K. Wilson and J. Kogut. *The renormalization Group and the Epsilon Expansion*. *Physics Reports*, 12:75–199, 1974.

[204] Y. Nishida and D. Son. *Epsilon Expansion for a Fermi Gas at Infinite Scattering Length*. *Physical Review Letters*, 97:050403, 2006.

[205] Y. Nishida and S.N. Tan. *Universal Fermi Gases in Mixed Dimensions*. *Physical Review Letters*, 101:170401, 2011.

[206] Richard C. Tolman. Static solutions of einstein's field equations for spheres of fluid. *Phys. Rev.*, 55:364–373, Feb 1939.

[207] J. R. Oppenheimer and G. M. Volkoff. On massive neutron cores. *Phys. Rev.*, 55:374–381, Feb 1939.

[208] Bin Hong, ZhongZhou Ren, Chen Wu, and XueLing Mu. Impacts of symmetry energy slope on the oscillation frequencies of neutron stars with short-range correlation and admixed dark matter. *Classical and Quantum Gravity*, 40(12):125007, May 2023.

[209] N. M. Hugenholtz and L. van Hove. A theorem on the single particle energy in a Fermi gas with interaction. *Physica*, 24(1):363–376, January 1958.

[210] Bao-Jun Cai and Lie-Wen Chen. Lorentz covariant nucleon self-energy decomposition of the nuclear symmetry energy. *Physics Letters B*, 711(1):104108, May 2012.

[211] Chang Xu, Bao-An Li, Lie-Wen Chen, and Che-Ming Ko. *Analytical Relations between Nuclear Symmetry Energy and Single-nucleon Potentials in Isospin Asymmetric Nuclear Matter*. *Nuclear Physics A*, 865:1–16, 2011.

[212] Jun Xu, Lie-Wen Chen, Bao-An Li, and Hong-Ru Ma. Locating the inner edge of the neutron star crust using terrestrial nuclear laboratory data. *Phys. Rev. C*, 79:035802, Mar 2009.

[213] James M. Lattimer and Maddapa Prakash. Neutron Star Observations: Prognosis for Equation of State Constraints. *Phys. Rept.*, 442:109–165, 2007.

[214] Sebastian Kubis. The nuclear symmetry energy and stability of matter in neutron star. *Phys. Rev. C*, 76:025801, 2007.

[215] Gordon Baym, Christopher Pethick, and Peter Sutherland. The Ground State of Matter at High Densities: Equation of State and Stellar Models. *apj*, 170:299, December 1971.

[216] Kei Iida and Katsuhiro Sato. Spin Down of Neutron Stars and Compositional Transitions in the Cold Crustal Matter. *apj*, 477(1):294–312, March 1997.

[217] Lucas A. Souza, Mariana Dutra, César H. Lenzi, and Odilon Lourenço. Effects of short-range nuclear correlations on the deformability of neutron stars. *Phys. Rev. C*, 101:065202, Jun 2020.

[218] Laura Tolos, Mario Centelles, and Angels Ramos. The equation of state for the nucleonic and hyperonic core of neutron stars. *Publications of the Astronomical Society of Australia*, 34, 2017.

[219] G. A. Lalazissis, J. König, and P. Ring. New parametrization for the lagrangian density of relativistic mean field theory. *Physical Review C*, 55(1):540543, January 1997.

[220] E H Rodrigues, M Dutra, and O Lourenço. Recent astrophysical observations reproduced by a short-range correlated van der waals-type model? *Monthly Notices of the Royal Astronomical Society*, 523(4):48594868, June 2023.

[221] J. M. Dong. Nucleon-nucleon short-range correlation, superfluidity and neutron star cooling. *European Physical Journal A*, 60(2):34, February 2024.

[222] X.L. Shang, P. Wang, W. Zuo, and J.M. Dong. Role of nucleon-nucleon correlation in transport coefficients and gravitational-wave-driven r-mode instability of neutron stars. *Physics Letters B*, 811:135963, December 2020.

[223] CX Liu, TF Feng, and J M Dong. Effects of nucleon-nucleon short-range correlation and symmetry energy on the evolution of newly born magnetars. *Monthly Notices of the Royal Astronomical Society*, 534(3):1763–1774, 09 2024.

[224] Lucas A. Souza, Rodrigo Negreiros, Mariana Dutra, Débora P. Menezes, and Odilon Lourenço. Short-range correlation effects on the neutron star cooling, 2020. arXiv:2004.10309.

[225] Bin Hong, Tongqi Liang, and Zhongzhou Ren. Nucleon-nucleon short-range correlations: A hidden driver in binary neutron star inspiral gravitational waves. *Phys. Lett. B*, 860:139225, 2025.

[226] Sakshi Gautam, Anagh Venneti, Sarmistha Banik, and B.K. Agrawal. Re-visiting the role of short-range correlations on neutron-star properties. *Nuclear Physics A*, 1053:122978, 2025.

[227] O. Lourenço, T. Frederico, and M. Dutra. Dark matter component in hadronic models with short-range correlations. *Physical Review D*, 105(2), January 2022.

[228] Odilon Lourenço, Everson H. Rodrigues, Carline Biesdorf, and Mariana Dutra. Effects of short-range correlations at high densities on neutron stars with and without dm content: role of the repulsive self-interaction, 2025. arXiv:2511.15693.

[229] Bin Hong, ZhongZhou Ren, and Xue-Ling Mu. Short-range correlation effects in neutron star's radial and non-radial oscillations *. *Chinese Physics C*, 46(6):065104, jun 2022.

[230] Bao-Jun Cai and Lie-Wen Chen. Constraints on the skewness coefficient of symmetric nuclear matter within the nonlinear relativistic mean field model. *Nuclear Science and Techniques*, 28(12), December 2017.

[231] Hao Lu, Zhongzhou Ren, and Dong Bai. Neutron-neutron short-range correlations and their impacts on neutron stars. *Nucl. Phys. A*, 1021:122408, 2022.

[232] Grigoris Panotopoulos and Ildio Lopes. Dark matter effect on realistic equation of state in neutron stars. *Phys. Rev. D*, 96:083004, Oct 2017.

[233] John Ellis, Gert Hütsi, Kristjan Kannike, Luca Marzola, Martti Raidal, and Ville Vaskonen. Dark matter effects on neutron star properties. *Phys. Rev. D*, 97:123007, Jun 2018.

[234] Ann Nelson, Sanjay Reddy, and Dake Zhou. Dark halos around neutron stars and gravitational waves. *JCAP*, 07:012, 2019.

[235] H. C. Das, Ankit Kumar, and S. K. Patra. Dark matter admixed neutron star as a possible compact component in the gw190814 merger event. *Phys. Rev. D*, 104:063028, Sep 2021.

[236] Hong-Ming Liu, Jin-Biao Wei, Zeng-Hua Li, G.F. Burgio, and H.-J. Schulze. Dark matter effects on the properties of neutron stars: Optical radii. *Physics of the Dark Universe*, 42:101338, 2023.

[237] Naibo Zhang, Bao-An Li, Jiayu Zhang, Weinan Shen, and Hui Zhang. Illuminating dark matter admixed in neutron stars with simultaneous mass-radius constraints. *Symmetry*, 17(10):1669, October 2025.

[238] Hongyi Sun and Dehua Wen. New criterion for the existence of dark matter in neutron stars. *Physical Review D*, 109(12), June 2024.

[239] Nirmal Raj, Philip Tanedo, and Hai-Bo Yu. Neutron stars at the dark matter direct detection frontier. *Phys. Rev. D*, 97:043006, Feb 2018.

[240] Raghuveer Garani and Julian Heeck. Dark matter interactions with muons in neutron stars. *Phys. Rev. D*, 100:035039, Aug 2019.

[241] Nicole F. Bell, Giorgio Busoni, Sandra Robles, and Michael Virgato. Improved treatment of dark matter capture in neutron stars. *Journal of Cosmology and Astroparticle Physics*, 2020(09):028028, September 2020.

[242] Nicole F Bell, Giorgio Busoni, Theo F Motta, Sandra Robles, Anthony W. Thomas, and Michael Virgato. Nucleon structure and strong interactions in dark matter capture in neutron stars. *Phys. Rev. Lett.*, 127:111803, Sep 2021.

[243] Xue-Zhi Liu, Premachand Mahapatra, Chun Huang, Ayush Hazarika, Chiranjeeb Singha, and Prasanta Kumar Das. Revealing dark matter's role in neutron stars anisotropy: A bayesian approach using multimessenger observations. *Phys. Rev. D*, 112:083032, Oct 2025.

[244] Maurício Hippert, Emily Dillingham, Hung Tan, David Curtin, Jacquelyn Noronha-Hostler, and Nicolás Yunes. Dark matter or regular matter in neutron stars? how to tell the difference from the coalescence of compact objects. *Physical Review D*, 107(11), June 2023.

[245] Ankit Kumar and Hajime Sotani. Constraints on the parameter space in dark matter admixed neutron stars. *Phys. Rev. D*, 110(6):063001, 2024.

[246] Premachand Mahapatra, Chiranjeeb Singha, Ayush Hazarika, and Prasanta Kumar Das. Implications of fermionic dark matter interactions on anisotropic neutron stars. *The Astrophysical Journal*, 985(1):74, May 2025.

[247] O. Hen, A. W. Steiner, E. Piasetzky, and L. B. Weinstein. Analysis of neutron stars observations using a correlated fermi gas model, 2016. arXiv:1608.00487.

[248] A. Abrikosov, L. Gorkov, and I. Dzyaloshinski. *Methods of Quantum Field Theory in Statistical Physics*. Dover Press, 1963, Chap.2, Chap.5.

[249] M. R. Pelicer, D. P. Menezes, M. Dutra, and O. Lourenço. Do short range correlations inhibit the appearance of the nuclear pasta? *The European Physical Journal A*, 59(9), September 2023.

[250] J. W. Negele and K. Yazaki. Mean free path in a nucleus. *Phys. Rev. Lett.*, 47:71–74, Jul 1981.

[251] D. Q. Fang, Y. G. Ma, and C. L. Zhou. Shear viscosity of hot nuclear matter by the mean free path method. *Phys. Rev. C*, 89:047601, Apr 2014.

[252] S. X. Li, D. Q. Fang, Y. G. Ma, and C. L. Zhou. Shear viscosity to entropy density ratio in the boltzmann-uehling-uhlenbeck model. *Phys. Rev. C*, 84:024607, Aug 2011.

[253] Jun Xu, Lie-Wen Chen, Che Ming Ko, Bao-An Li, and Yu Gang Ma. Shear viscosity of neutron-rich nucleonic matter near its liquidgas phase transition. *Physics Letters B*, 727(13):244248, November 2013.

[254] C. L. Zhou, Y. G. Ma, D. Q. Fang, and G. Q. Zhang. Thermodynamic properties and shear viscosity over entropy-density ratio of the nuclear fireball in a quantum-molecular dynamics model. *Phys. Rev. C*, 88:024604, Aug 2013.

[255] Cong Liu, Xian-Gai Deng, and Yu-Gang Ma. Density fluctuations in intermediate-energy heavy-ion collisions. *Nucl. Sci. Tech.*, 33(5):52, 2022.

[256] Xian-Gai Deng, De-Qing Fang, and Yu-Gang Ma. Shear viscosity of nucleonic matter. *Progress in Particle and Nuclear Physics*, 136:104095, March 2024.

[257] Yu-Gang Ma, Long-Gang Pang, Rui Wang, and Kai Zhou. Phase transition study meets machine learning. *Chinese Physics Letters*, 40(12):122101, December 2023.

[258] X. G. Deng, P. Danielewicz, Y. G. Ma, H. Lin, and Y. X. Zhang. Impact of fragment formation on shear viscosity in the nuclear liquid-gas phase transition region. *Phys. Rev. C*, 105:064613, Jun 2022.

[259] X. G. Deng, Y. G. Ma, and M. Veselský. Thermal and transport properties in central heavy-ion reactions around a few hundred mev/nucleon. *Phys. Rev. C*, 94:044622, Oct 2016.

[260] Arnau Rios, Artur Polls, and W. H. Dickhoff. Depletion of the nuclear Fermi sea. *Phys. Rev. C*, 79:064308, 2009.

[261] Omar Benhar, Donal Day, and Ingo Sick. Inclusive quasielastic electron-nucleus scattering. *Rev. Mod. Phys.*, 80:189–224, Jan 2008.

[262] L. Shi and P. Danielewicz. Effect of cluster formation on isospin asymmetry in the liquid gas phase transition region. *EPL*, 49:34–40, 2000.

[263] Bao-An Li, Lie-Wen Chen, and Che-Ming Ko. *Recent Progress and New Challenges in Isospin Physics with Heavy-ion Reactions*. *Physics Reports*, 464:113–281, 2008.

[264] Jie Zhao, Jin-Hui Chen, Xu-Guang Huang, and Yu-Gang Ma. Electromagnetic fields in ultra-peripheral relativistic heavy-ion collisions. *Nuclear Science and Techniques*, 35(2), February 2024.

[265] Xin Wu, Xin-Bai Li, Ze-Bo Tang, Kai-Yang Wang, and Wang-Mei Zha. Impact parameter manipulation in exclusive photoproduction in Electron-Ion Collisions. *Nuclear Science and Techniques*, 36(9):157, September 2025.

[266] Z. X. Yang, X. L. Shang, G. C. Yong, W. Zuo, and Y. Gao. Nucleon momentum distributions in asymmetric nuclear matter. *Phys. Rev. C*, 100(5):054325, 2019.

[267] J. Carriere, C. J. Horowitz, and J. Piekarewicz. Lowmass neutron stars and the equation of state of dense matter. *The Astrophysical Journal*, 593(1):463471, August 2003.

[268] A. S. Schneider, C. J. Horowitz, J. Hughto, and D. K. Berry. Nuclear pasta formation. *Physical Review C*, 88(6), December 2013.

[269] M. E. Caplan and C. J. Horowitz. Colloquium: Astromaterial science and nuclear pasta. *Rev. Mod. Phys.*, 89:041002, Oct 2017.

[270] William G. Newton, Sarah Cantu, Shuxi Wang, Amber Stinson, Mark Alexander Kaltenborn, and Jirina Rikovska Stone. Glassy quantum nuclear pasta in neutron star crusts. *Physical Review C*, 105(2), February 2022.

[271] Rui Wang, Zhen Zhang, Yu-Gang Ma, Lie-Wen Chen, Che Ming Ko, and Kai-Jia Sun. Alpha clustering in warm and dense nuclear matter from heavy-ion collisions, 2025. arXiv:2507.16613.

[272] Bo Zhou, Yasuro Funaki, Hisashi Horiuchi, and Akihiro Tohsaki. Nonlocalized clustering and evolution of cluster structure in nuclei. *Frontiers of Physics*, 15(1), August 2019.

[273] Xiao-Quan Du, Cong-Wu Wang, De-Ye Tao, Bo Zhou, and Yu-Gang Ma. Dineutron and diproton correlations in the exotic nuclei 6He and 6Be . *Nuclear Science and Techniques*, 36(11):205, August 2025.

[274] De-Ye Tao and Bo Zhou. Reduced-width amplitude in nuclear cluster physics. *Nucl. Sci. Tech.*, 36(4):56, 2025.

[275] Kang Wei, Yan-Lin Ye, and Zai-Hong Yang. Clustering in nuclei: progress and perspectives. *Nuclear Science and Techniques*, 35(12):216, December 2024.

[276] Xin-Yu Xu, Si-Qin Fan, Qi Yuan, Bai-Shan Hu, Jian-Guo Li, Si-Min Wang, and Fu-Rong Xu. Progress in ab initio in-medium similarity renormalization group and coupled-channel method with coupling to the continuum. *Nucl. Sci. Tech.*, 35(12):215, 2024.

[277] PJ. Siemens and H. Bethe. *Shape of Heavy Nuclei*. *Physical Review Letters*, 18:704–706, 1967.

[278] Cheuk-Yin Wong. *Toroidal Nuclei*. *Physics Letters B*, 41:446–450, 1972.

[279] Cheuk-Yin Wong. *Toroidal and Spherical Bubble Nuclei*. *Annals of Physics*, 77:279–353, 1973.

[280] Xi-Guang Cao and et al. *Examination of Evidence for Resonances at High Excitation Energy in the 7-alpha Disassembly of ^{28}Si* . *Physical Review C*, 99:014606, 2019.

[281] J. B. Natowitz, G. Röpke, S. Typel, D. Blaschke, A. Bonasera, K. Hagel, T. Klähn, S. Kowalski, L. Qin, S. Shlomo, R. Wada, and H. H. Wolter. Symmetry energy of dilute warm nuclear matter. *Phys. Rev. Lett.*, 104:202501, May 2010.

[282] Sanjay Reddy, Madappa Prakash, and James M. Lattimer. Neutrino interactions in hot and dense matter. *Phys. Rev. D*, 58:013009, May 1998.

[283] Sanjay Reddy, Madappa Prakash, James M. Lattimer, and Jose A. Pons. Effects of strong and electromagnetic correlations on neutrino interactions in dense matter. *Phys. Rev. C*, 59:2888–2918, May 1999.

- [284] Chang-Feng Jiao and Cen-Xi Yuan. The impact of tensor force on collective correlations and neutrinoless double- β decay. *Nuclear Science and Techniques*, 36(11):202, August 2025.
- [285] Brian D. Serot. A relativistic nuclear field theory with and mesons. *Physics Letters B*, 86(2):146–150, 1979.
- [286] Bao-Jun Cai, Farrukh J. Fattoyev, Bao-An Li, and William G. Newton. Critical density and impact of $\Delta(1232)$ resonance formation in neutron stars. *Phys. Rev. C*, 92:015802, Jul 2015.
- [287] Jin-Hui Chen, Feng-Kun Guo, Yu-Gang Ma, Cheng-Ping Shen, Qi-Ye Shou, Qian Wang, Jia-Jun Wu, and Bing-Song Zou. Production of exotic hadrons in pp and nuclear collisions: Production of exotic hadrons in pp and nuclear collisions. *Nuclear Science and Techniques*, 36(4):55, April 2025.
- [288] Dong-Fang Wang, Mei-Yi Chen, Yu-Gang Ma, Qi-Ye Shou, Song Zhang, and Liang Zheng. Investigating the pion emission source in pp collisions using the AMPT model with subnucleon structure. *Nuclear Science and Techniques*, 36(8):154, August 2025.
- [289] Kenji Fukushima, Josuke Minamiguchi, and Tomoya Uji. Magnetic-type love number differentiating quark stars from neutron stars, 2025. arXiv:2511.02236.